PHYSICAL REVIEW B **81**, 224205 (2010)

Generalization of the cavity method for adiabatic evolution of Gibbs states

Lenka Zdeborová[1] and Florent Krzakala[2,1]
[1]*Theoretical Division and Center for Nonlinear Studies, Los Alamos National Laboratory, Los Alamos, New Mexico 87545, USA*
[2]*ESPCI Paris Tech, CNRS UMR 7083 Gulliver, 10 rue Vauquelin, Paris 75005, France*
(Received 24 February 2010; revised manuscript received 12 May 2010; published 10 June 2010)

Mean-field glassy systems have a complicated energy landscape and an enormous number of different Gibbs states. In this paper, we introduce a generalization of the cavity method in order to describe the adiabatic evolution of these glassy Gibbs states as an external parameter, such as the temperature, is tuned. We give a general derivation of the method and describe in details the solution of the resulting equations for the fully connected *p*-spin model, the XOR-satisfiability (SAT) problem and the antiferromagnetic Potts glass (coloring problem). As direct results of the states following method we present a study of very slow Monte Carlo annealings, the demonstration of the presence of temperature chaos in these systems and the identification of an easy/hard transition for simulated annealing in constraint optimization problems. We also discuss the relation between our approach and the Franz-Parisi potential, as well as with the reconstruction problem on trees in computer science. A mapping between the states following method and the physics on the Nishimori line is also presented.

DOI: 10.1103/PhysRevB.81.224205 PACS number(s): 64.70.qd, 75.50.Lk, 89.70.Eg

I. INTRODUCTION

Both in classical and quantum thermodynamics, it is often practical to discuss very slow variations in an external parameter so that the system remains at equilibrium and such very slow changes are referred to as adiabatic.[1] When a macroscopic system is in a given phase and if one tunes a parameter, say the temperature, very slowly then all observables, such as the energy or the magnetization in a magnet, will be given by the equilibrium equation of state.

Such considerations have to be revisited close to a phase transition where it is impossible to be truly adiabatic and this is the subject of modern out-of-equilibrium theories. However, given a system at equilibrium in a well-defined phase, it is always possible to consider the adiabatic evolution. In the low-temperature phases of a ferromagnet, for instance, the evolution of the magnetization is different in the two phases (or Gibbs states) corresponding to the positive or negative magnetization. To describe this theoretically, one can force the system to be in the Gibbs state of choice (for instance, by adding an external infinitesimal field or fixing the boundary conditions) and then study the adiabatic evolution for each of these phases.

This simplicity, however, breaks when one considers glassy systems where the energy landscape is very complicated and especially in the mean-field setting where an exponential number of phases (Gibbs states) exists. Adiabatic evolution of phases in mean-field glassy systems is, however, a very important problem that has been considered—via some approximation or in very specific solvable cases—in a number of works.[2–9] How to deal with this situation in general mean-field glassy systems, how to chose a particular phase, and how to follow it adiabatically is the subject of the formalism presented in this work.

Mean-field glassy systems are important in many parts of modern science. We shall call a system a *mean-field* one whenever a mean-field treatment is exact for this system: this is the case for all spin or particle models on fully connected lattices (such as the Curie-Weiss model of ferromagnets) or on sparse random lattices that are locally treelike (such as the Bethe lattice). Over the last few years, studies of mean-field glassy systems brought many interesting results in physics as well as in computer science. Without being exhaustive, we can mention the development of mean-field theories for structural glass formers[10,11] for the jamming transition and amorphous packing,[12] heteropolymer folding,[13] or for quantum-disordered materials[14] on the physics side. On the computer science side, many results have been obtained using mean-field theory on optimization problems and neural network,[15] and more recently random constraint satisfaction problems have witnessed a burst of new results via the application of the survey propagation algorithm and related techniques.[16,17] The theory of error-correcting codes is also closely related to glassy mean-field system,[18] etc.

A common denominator in all these systems is their complex energy landscape and a large number of phases (states), whose statistical features are amenable to an analytical and quantitative description via the replica and cavity methods.[15,19] However, important and deep questions about the dynamical behavior in these systems remain largely unsolved and many of them can be addressed by the knowledge of the slow dynamics. In order to motivate our approach, let us first discuss the basic universal features of the thermodynamic behavior of mean-field glassy models. As an external parameter, say the temperature T, is tuned, a typical glassy system undergoes the following changes: at high temperature, the system is in a paramagnetic/liquid phase. Below the *dynamical* glass temperature T_d, this phase shatters into exponentially many Gibbs states/phases, all well separated by extensive energetic or entropic barriers, leading to a breaking of ergodicity and to the divergence of the equilibration time.[2,20,21] As the temperature is further lowered, the number of states (relevant for the Boltzmann measure) may become finite and the structural entropy (or complexity) vanishes, this defines the *static* Kauzmann transition, T_K, arguably similar to the one observed in real glass formers.[11,22] This

scenario is called the *one-step replica symmetric* (1RSB) picture. In some models,[23] the states will divide further into an infinite hierarchy of substates, a phenomenon called *full replica symmetry breaking* (FRSB).[15,19]

The 1RSB picture is well established in many mean-field systems and the cavity/replica method is able to compute the number, the size, or the energy of the equilibrium Gibbs states. However, with the exception of few simple models,[2,3,6–9] an analytical description of the dynamics and of the way states are evolving upon adiabatic change in external parameters is missing. Let us consider a given setting where the need for adiabatic following is clear. Imagine an annealing experiment where the temperature T is changed in time as $T=T_0-\delta t/N$. Take the thermodynamic limit $N\to\infty$ first and then consider a very slow annealing $\delta\to 0$. As long as we stay in the paramagnetic phase, we expect that such a slow annealing will equilibrate. The fact that the equilibration time is finite above T_d can be actually proven[21,24] and such slow annealings should be thus able to equilibrate down to the dynamical temperature T_d after which the system gets stuck in one of the many equilibrium Gibbs states. Computing the energy of the lowest configuration belonging to this state would thus give the limiting energy for a very slow annealing (and thus would give a bound to the performance of any annealing scheme). However, while the standard cavity and the replica methods predict all the properties of an *equilibrium* state at a given temperature T_e (equilibrium temperature), they do not tell how these properties change *for this precise state* when the temperature changes adiabatically to $T_a\neq T_e$ (actual temperature). A word of caution: we want to follow the state and stay in it. Hence by *adiabatic* we mean here slow only *linearly* in the size of the system, corresponding to very long experimental times; an *exponentially* slow annealing always finds the ground state, but this is of course unfeasibly long.

The extension of the cavity method that we introduced in a recent letter[25] precisely answered these questions by following adiabatically the evolution of any Gibbs state when an external parameter is changed (for an intuitive and pictorial description of our goals, see Fig. 1). This method gives detailed quantitative information about the energy landscape and the long-time dynamics. The aim of this subsequent publication is to derive the method in general, to discuss in detail the solutions of the resulting equations, and to discuss relations with some other settings (reconstruction on trees,[26] Franz-Parisi potential,[27,28] and Nishimori line[29]). We anticipate that the method will become part of the standard toolbox for mean-field glassy systems and hence a detailed presentation is appropriate.

The paper is organized as follow: in Sec. II we give a brief reminder of the usual cavity method. In the next two sections, we present our formalism for the adiabatic evolution of states from temperature higher (Sec. III) and lower (Sec. IV) than the spin-glass static/Kauzmann transition. We finally solve these equations and present our results for a fully connected model in Sec. V and for diluted models on the Bethe lattice in Sec. VI.

II. PRELIMINARIES

In this section, we first review the results of the standard cavity method that we shall use all along the text. The specific example for which we shall derive most of the results of this paper is the p-spin model, also called the XOR-SAT problem. However, the derivation for all other models where the cavity method[19] can be used goes in the very same lines (and we will also work later on with the coloring problem). The reader familiar with the cavity method can skip this section and go directly to Sec. III.

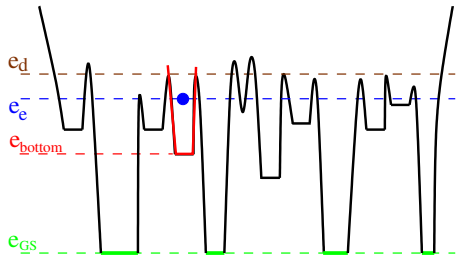

FIG. 1. (Color online) A cartoon of the energy landscape in mean-field glassy systems. The different valleys correspond to different Gibbs states and are separated by extensive barriers. For energies lower than e_d (the uppermost brown line), ergodicity breaks because of these barriers. The ground-state energy of the system is $e_{\rm GS}$ (the lowermost green line). The standard cavity and replica method can compute how many states of a given size/entropy are present at a given energy/temperature e/T. The states following method we develop in this paper instead pins down one state (in red, marked by the point, in the figure) that is one of the equilibrium ones at energy e_e (corresponding to temperature T_e, the blue line with a point) and computes its properties (entropy, energy) for another temperatures T_a: we are thus *following* a given state as temperature (or any other parameter) is changed. At $T_a=0$, this leads, for instance, to the properties of the bottom of the state as, e.g., the limiting energy $e_{\rm bottom}$.

A. p-spin model and XOR-SAT reminder

The p-spin model is defined by its Hamiltonian

$$\mathcal{H}=-\sum_a J_a\prod_{i\in\partial a} s_i, \tag{1}$$

where $s_i\in\{-1,+1\}$ are the Ising spins, a are interactions between p uples of spins, and J_a is the strength of the interaction.

In what follows we will focus on two cases of the p-spin model:

(a) XOR-SAT (parity check) problem: in this case all the interactions $|J_a|=1$. The interactions can be both ferromagnetic and antiferromagnetic,

$$Q(J_a)=\rho\delta(J_a+1)+(1-\rho)\delta(J_a-1). \tag{2}$$

In Sec. V and VI we mostly consider the spin-glass case $\rho=1/2$. The number of interactions M (linear equations) is $M=\alpha N$, where α is the constraints density. The degree distribution $\mathcal{Q}(l)$ of variables has to be specified here. The number of violated parity checks (constraints) is $E=(M+\mathcal{H})/2$. The values of temperature for the K-XOR-SAT problems are hence related to those for the p-spin problem via a multiplicative factor 2, note that here and throughout the paper $K=p$.

(b) Fully connected p-spin model: the interactions a exist for every possible p uple of spins, the mean and variance of J_a are given by $\langle J_a\rangle = J_0 p!/N^{p-1}$ and $\langle J_a^2\rangle - \langle J_a\rangle^2 = J^2 p!/(2N^{p-1})$.

The XOR-SAT problem was studied and solved in Refs. 30–33, and its most important application are the low-density parity check error correcting codes.[34,35] The fully connected p-spin model was introduced in Refs. 36 and 37 and now stands at the root of the random first-order theory of the glass transition.[10,38,39]

In our examples we will mainly use the ensemble of random regular graphs, i.e., $\mathcal{Q}(l)=\delta(c-l)$ and obtain the fully connected limit by taking $c\to\infty$. The formulas are, however, written mostly for a general degree distribution (with a finite second moment). In the cavity equations we often need the excess degree distribution, that is the probability distribution of the number of excess edges given one edge is chosen, that is (denoting $\bar{l}$ the average coordination number),

$$q(l) = \frac{(l+1)\mathcal{Q}(l+1)}{\bar{l}}. \tag{3}$$

1. Liquid phase: Belief propagation equations

We now summarize in a very brief manner and without extensive derivations the known cavity equations for the XOR-SAT problem as we are going to need them for derivation of the states following method. We are trying to keep the equations in the most general form such that generalizations to other models are straightforward. The very principle of the cavity method is that we are working with treelike graphs. Random graphs are locally a tree and we thus can work "as if" on a tree (we will eventually have to consider the boundary conditions and precise the relation to random graphs later on). Solving the problem on a tree can be done easily with a recursive procedure that was introduced by Bethe.[40] We will, however, use the modern language of computer science, where this method is called belief propagation (BP).

For the XOR-SAT problem the BP equations read

$$\chi_{s_i}^{i\to a} = \frac{1}{Z_\chi^{i\to a}(\{\psi^{b\to i}\},\beta)} \prod_{b\in\partial i\backslash a} \psi_{s_i}^{b\to i}, \tag{4}$$

$$\psi_{s_i}^{b\to i} = \frac{1}{Z_\psi^{b\to i}(\{\chi^{j\to b}\},\beta)} \sum_{\{s_j\}} e^{\beta J_b \prod_{j\in\partial b} s_j} \prod_{j\in\partial b\backslash i} \chi_{s_j}^{j\to b}, \tag{5}$$

where $Z_\psi^{b\to i}$ and $Z_\chi^{i\to a}$ are normalizations ensuring that $\psi_{+1}^{b\to i}+\psi_{-1}^{b\to i}=1$ and $\chi_{+1}^{i\to a}+\chi_{-1}^{i\to a}=1$. The quantities $\chi_{s_i}^{i\to a}$ (respectively, $\psi_{s_i}^{b\to i}$) are interpreted in terms of messages being send from a variable i to a constraint a (respectively, from constraint b to variable i) (see Fig. 2 for a pictorial representation with the so-called *factor graph*). Message $\chi_{s_i}^{i\to a}$ is a probability that variable i takes value s_i conditioned on constraint a to be missing from the graph. Message $\psi_{s_i}^{b\to i}$ is a probability that the constraint b is satisfied given that variable i takes values s_i. The recursion could also be written with one single type of message as

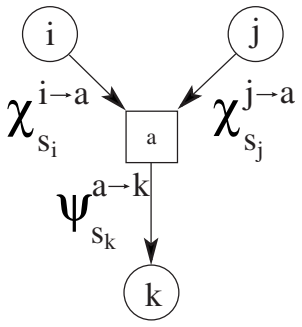

FIG. 2. A sketch of the basic cavity recursion in the factor graph representation of XOR-SAT. The square represents a constraint involving the product of three spins while the circles represent the spin variables. The message passing procedure called belief propagation uses messages from constraints to variables (ψ) and from variables to constraints (χ).

$$\psi_{s_i}^{a\to i} = \mathcal{F}(\{\psi^{b\to j}\},\beta) = \sum_{\{s_j\}} \frac{e^{\beta J_a s_i \prod_{j\in\partial a\backslash i} s_j}}{Z^{a\to i}(\{\psi^{b\to j}\},\beta)} \prod_{j\in\partial a\backslash i} \prod_{b\in\partial j\backslash a} \psi_{s_j}^{b\to j}$$
$$= \sum_{\{s_j\}} P(\{s_j\}|\{\psi^{b\to j}\},\beta,s_i). \tag{6}$$

Given all the messages computed on a given graph, one can compute the Bethe estimate of the free energy, which is also called the RS free energy,

$$-\beta F = \sum_a \log Z^{a+\partial a} - \sum_i (l_i-1)\log Z^i, \tag{7}$$

where the contributions to the free energy are

$$Z^{a+\partial a}(\{\psi^{b\to i}\},\beta) = \sum_{\{s_i\}} e^{\beta J_a \prod_{i\in\partial a} s_i} \prod_{i\in\partial a} \prod_{b\in\partial i-a} \psi_{s_i}^{b\to i}, \tag{8}$$

$$Z^i(\{\psi^{a\to i}\},\beta) = \prod_{a\in\partial i} \psi_{-1}^{a\to i} + \prod_{a\in\partial i} \psi_{+1}^{a\to i}. \tag{9}$$

By deriving the free energy with respect to the inverse temperature, we obtain the energy

$$E = \frac{\partial(\beta F)}{\partial\beta} = \sum_a E^{a+\partial a}(\{\psi^{b\to i}\},\beta)$$
$$= \sum_a \frac{\sum_{\{s_i\}} J_a \prod_{i\in\partial a} s_i e^{\beta J_a \prod_{i\in\partial a} s_i} \prod_{i\in\partial a} \prod_{b\in\partial i-a} \psi_{s_i}^{b\to i}}{\sum_{\{s_i\}} e^{\beta J_a \prod_{i\in\partial a} s_i} \prod_{i\in\partial a} \prod_{b\in\partial i-a} \psi_{s_i}^{b\to i}}. \tag{10}$$

All the above equations are written for a given instance (graph or given instance of the disorder) of the problem. It is often desirable to write the BP equations directly in the average form over the graph and disorder ensemble. This is the replica symmetric cavity equation,

$$P(\psi) = \sum_{\{l_i\}} q(\{l_i\}) \int \prod_{i=1}^{K-1} \prod_{j=1}^{l_i} dP(\psi^j)\, \delta[\psi - \mathcal{F}(\{\psi^j\},\beta)], \tag{11}$$

that can be solved numerically via the population dynamics technique introduced in Ref. 19 (see also Ref. 18 and 41 for details).

Whether the BP equations for XOR-SAT are solved on a given random graph or in the population dynamics, they have always the following fixed point that corresponds to the paramagnetic/liquid phase,

$$\psi^{a\to i}_{+1} = \psi^{a\to i}_{-1} = \chi^{i\to a}_{+1} = \chi^{i\to a}_{-1} = \frac{1}{2}, \tag{12}$$

for all i and a. Plugging this solution in the expression for the free energy we get

$$-\beta f = -\beta F/N = \frac{\bar{l}}{K}\log(\cosh\beta) + \log 2 \tag{13}$$

and for the energy we get

$$e = E/N = -\frac{\bar{l}}{K}\tanh\beta. \tag{14}$$

Hence, in this case, the probability that a given constraint is not satisfied is

$$\epsilon(\beta) = \frac{1}{1+e^{2\beta}}. \tag{15}$$

2. Glassy solution: One-step replica symmetry breaking

The replica symmetric liquid solution from the previous section is asymptotically exact as long as the point-to-set correlation length stays finite.[21] This is related to the reconstruction problem on trees.[26] When the point-to-set correlation length diverges, the replica symmetry-broken solution[19] has to be used to describe correctly the system.

In the one-step replica symmetry breaking one splits the phase space into exponentially many Gibbs states, $P^{a\to i}(\psi^{a\to i})$ is then the probability distribution over states of the cavity message $\psi^{a\to i}$. We now need to consider all these states and in order to focus on those with a given free energy $f=-T\log(Z)$, we weight them according to their partition function to a given power Z^x, where x is the so-called Parisi parameter. In the cavity method, x is then used as a Legendre parameter in order to select the states with a given free energy. With this in mind, the 1RSB self-consistent recursive equation reads[19]

$$P^{a\to i}(\psi^{a\to i}) = \frac{1}{\mathcal{Z}^{a\to i}(\beta)} \int \prod_{j\in\partial a\setminus i} \prod_{b\in\partial j\setminus a} dP^{b\to j}(\psi^{b\to j}) \times [Z^{a\to i}(\{\psi^{b\to j}\},\beta)]^x \delta[\psi^{a\to i} - \mathcal{F}(\{\psi^{b\to j}\},\beta)] \tag{16}$$

with $\mathcal{F}(\{\psi^{b\to j}\},\beta)$ and $Z^{a\to i}(\{\psi^{b\to j}\},\beta)$ being defined in Eq. (6). The Parisi parameter x is indeed a Legendre parameter conjugated to the internal free energy of states. The entropy associated with the number of states of a given internal free energy f, also called complexity and defined by $\Sigma(f) = \log[\mathcal{N}_{\text{states}}(f)]/N$, can be recovered from the following Legendre transform:

$$-\beta x\Phi(\beta,x) = -\beta x f(\beta) + \Sigma(f), \quad f(\beta) = \frac{\partial[x\Phi(\beta,x)]}{\partial x}. \tag{17}$$

The potential $\Phi(\beta,x)$ is computed from the fixed point of the 1RSB Eq. (16) as

$$\Phi(\beta,x) = \sum_a \Phi^{a+\partial a} - \sum_i (l_i - 1)\Phi^i, \tag{18}$$

where

$$e^{-\beta x\Phi^{a+\partial a}} = \int \prod_{i\in\partial a} \prod_{b\in\partial i\setminus a} dP^{b\to i}(\psi^{b\to i}) [Z^{a+\partial a}(\{\psi^{b\to i}\},\beta)]^x, \tag{19}$$

$$e^{-\beta x\Phi^{i}} = \int \prod_{a\in\partial i} dP^{a\to i}(\psi^{a\to i}) [Z^{i}(\{\psi^{a\to i}\},\beta)]^x. \tag{20}$$

The condition for validity of the replica symmetric solution is recovered by solving the 1RSB equations for $x=1$, that is if at $x=1$ there exists a nontrivial solution of Eq. (16) then the RS solution is not correct and the phase space needs to be divided into states. This happens at the dynamical temperature T_d.

The 1RSB solution is then given by the value of x such that

$$x^* = \text{argmax}_x[-\beta f(\beta) + \Sigma(f) | \Sigma(f) \geq 0]. \tag{21}$$

Above the Kauzmann temperature T_K one has $x^*=1$ and $\Sigma(f)>0$, that is, exponentially many states are relevant to the Boltzmann measure. In this phase the local magnetization (marginal probabilities) and the thermodynamic potentials, such as the total free energy, are still given by the replica symmetric solution, Eqs. (12)–(15).

Below the Kauzmann temperature $x^*<1$ and $\Sigma(f)=0$, the Boltzmann measure is dominated by only a finite number of states. However, an exponential numbers of subdominant (nonequilibrium) states still exist at any positive temperature.

B. Coloring of graphs, alias the antiferromagnet Potts model

We shall also illustrate some of our results on the antiferromagnetic Potts model on random graphs, mostly known and studied in its zero-temperature version since it is then equivalent to the graph coloring problem.[41–45] The Hamiltonian is

$$H = \sum_{(ij)\in G} \delta_{s_i,s_j}, \tag{22}$$

where s_i are Potts spins taking one of the q possible values (colors), $\delta_{i,j}$ is the Kronecker delta symbol, and the sum is

over all edges of the graph. The phase diagram of this model at finite temperature is summarized in Ref. 46 and all the necessary equations for both the replica symmetric and glassy solution can be found in Ref. 41.

III. EVOLUTION OF STATES ABOVE THE KAUZMANN TEMPERATURE

In this section we introduce the states following formalism and derive equations for the evolution of states that are at equilibrium above the Kauzmann temperature, $T_e \geq T_K$. In this phase, the paramagnetic replica symmetric solution, Eqs. (12)–(15), correctly describes all thermodynamic quantities (but misses the ergodicity breaking at $T_e < T_d$). In Sec. IV we give a generalization for equilibrium states below T_K and for metastable states.

In order to get an intuitive idea of what we will do, let us consider the ferromagnetic Ising model on a random graph. At low temperature, there are two phases corresponding to the positive and negative magnetization. In order to study one of these phases, a good strategy is to first recognize that the random graph is locally a tree. Then one considers a tree where all spins on the boundaries are fixed to, say, a value $s=1$, then far away from the boundaries the system will be in the phase of positive magnetization. By changing the temperature the curve $m^+(T)$ can be computed. We will follow the same strategy, except that choosing the correct boundaries will be slightly more involved.

The main idea behind the equations of state following is that we pick a configuration at random among the equilibrium ones at a temperature T_e and then we look at the solution of the belief propagation equations at a temperature T_a initialized in that configuration. We will also discuss a special case of factorized replica symmetric solution where this idea can be actually performed on a single graph. This is also closely related to the quiet planting discussed in Refs. 47 and 48.

A. Gedanken experiment on infinite trees

Let us consider the problem on a large hypertree. Let the hypertree have the same distribution of disorder (i.e., the degree distribution, the distribution of negations, interaction strengths, etc.) as the original problem. Let us consider a measure uniform over all configurations having energy corresponding to a given temperature T_e. To sample uniformly one configuration from this measure the following steps need to be done:

(a) take a much larger hypertree and start with random messages on the boundary of the larger hypertree and iterate the belief propagation equations at temperature T_e down to the root. This way one created messages taken from the replica symmetric solution on the original hypertree.

(b) Assign a value to the root according to the incoming message. Proceed iteratively up to the leaves of the hypertree with the following: given the value s_i of variable i choose the set of values $\{s_j\}$ according to probability $P(\{s_j\}|\{\psi^{b\to j}\},\beta_e,s_i)$ defined in Eq. (6), where a is a descendant of i and $b \in \partial j \backslash a$, for each $j \in \partial a \backslash i$.

Now consider the values of variables from the configuration, we picked on the leaves. This is a boundary condition that defines the equilibrium Gibbs state at temperature T_e (as long as $T_e \geq T_K$). Next consider the belief propagation equations at temperature $T_a \neq T_e$, initialize the messages on the leaves of the hypertree in the configuration we picked (i.e., $\psi_s=1$ and $\psi_r=0$ for all $r \neq s$ if we picked value s) and iterate down to the root. The result of these iterations describes properties (free energy, energy, size, overlap) of the Gibbs state at the temperature $T_a \neq T_e$.

In case the original temperature was above the dynamical glass temperature, $T_e > T_d$, the solution of the belief propagation at T_a will not be different from the result of the pure BP at T_a. That is because all the equilibrium configurations above T_d lie in the same paramagnetic state.

When the original temperature is below the dynamical glass temperature, $T_K \leq T_e \leq T_d$, the situation is much more interesting. Then the equilibrium configuration we picked lies in one of the exponentially many equilibrium Gibbs states and the belief propagation equations at a different temperature do describe adiabatic evolution of that Gibbs state. In what follows we shall translate the above reasoning into the cavity equations and describe the population dynamics technique used to solve them.

B. Simplest case: Factorized RS solution

The simplest form of the equations for adiabatic evolution of states can be written when the replica symmetric solution is *factorized*, i.e., when the values of the messages are the same. This is the case in the XOR-SAT problem where there is a BP fixed point in which for all i and a the message $\psi^{a\to i}=1/2$. Furthermore, this fixed point gives an asymptotically exact results above the Kauzmann temperature T_K.

When the RS solution is factorized, the step (a) in the construction of the equilibrium configuration can be skipped and the probabilities $P(\{s_j\}|\{\psi^{b\to j}\},\beta_e,s_i)$ depend only on the values of variables and the inverse temperature β_e. In the XOR-SAT, in particular, we have from Eq. (6),

$$P(\{s_j\}|\{\psi^{b\to j}\},\beta_e,s_i) = \frac{e^{\beta_e J_a s_i \prod_{j\in\partial a\backslash i} s_j}}{2^{K-1}\cosh(\beta_e J_a)}. \tag{23}$$

Meaning that a clause is unsatisfied with probability $\epsilon(\beta_e)$ that is given by Eq. (15). These probabilities are used according to step (b) to choose an equilibrium configuration on the hypertree. Then belief propagation equations at a temperature T_a are initialized on the leaves in that configuration and iterated. As usual for belief propagation equations a probability distribution of the values of messages can be written. This time one has to distinguish between messages sent to the variables which were assigned value +1 in the equilibrium configuration and those that were assigned −1. Given the probabilities to choose values of variables, Eq. (23), the two probability distributions have to satisfy the following self-consistent equation,

$$P_s(\psi) = \sum_J Q(J) \sum_{\{l_i\}} q(\{l_i\}) \sum_{\{s_i\}} \frac{e^{J\beta_e s \prod_i s_i}}{2^{K-1} \cosh \beta_e J} \times \int \prod_{i=1}^{K-1} \prod_{j=1}^{l_i} dP_{s_i}(\psi^j) \delta[\psi - \mathcal{F}(\{\psi^j\}, \beta_a)], \quad (24)$$

where $q(\{l_i\})$ is the excess degree distribution and $\mathcal{F}(\{\psi^j\}, \beta_a)$ is defined in Eq. (6). Note the use of inverse temperature β_a in the BP equations represented by the delta function. Given a Gibbs state that is one of the equilibrium ones at temperature T_e, Eq. (24) encodes its properties when the temperature is changed to T_a.

The learned reader will recognize that when $T_e = T_a$ this is nothing but the 1RSB equation[26] (at Parisi parameter $x=1$). This is actually quite normal: since when the two temperatures are equal we are just describing the properties of a typical state, which is what the 1RSB method does. Similar equations when the two temperatures are equal were thus considered in many works.[41,47,49,50]

To solve Eq. (24) with the population dynamics we represent $P_s(\psi)$ by an array of values for each value of s. To update one element in the array P_s we first pick degrees l_i from the excess degree distribution, then based on value of s and Eq. (23) we pick the values $\{s_i\}$. After that, for each i we pick l_i random elements in the array P_{s_i} and based on Eq. (6) we compute a new value of ψ and replace one element in the array P_s. We repeat many times until (based on computation of some average quantities) the convergence is reached. It is also important to note that the initial state of the populations corresponding to the boundary conditions on the hypertree is

$$P_s(\psi) = \delta\left[\begin{pmatrix} \psi_s \\ \psi_{-s} \end{pmatrix} - \begin{pmatrix} 1 \\ 0 \end{pmatrix}\right]. \quad (25)$$

The internal Bethe free energy of the state is

$$-\beta_a f(\beta_a) = \alpha \sum_J Q(J) \sum_{\{l\}} q(\{l\}) \sum_{\{s_i\}} \frac{e^{J\beta_e s \prod_i s_i}}{2^K \cosh \beta_e J} \times \int \prod_{i=1}^{K} \prod_{j=1}^{l_i} [d\psi^j P_{s_i}^j(\psi^j)] \log Z^{a+\partial a}(\{\psi^j\}, \beta_a) - \sum_l \mathcal{Q}(l) \frac{l-1}{2} \sum_{s_i} \int \prod_{i=1}^{l} [d\psi^j P_{s_i}^i(\psi^j)] \times \log Z^i(\{\psi^j\}, \beta_a). \quad (26)$$

The value can be computed using the population dynamics procedure based on the fixed point of Eq. (24).

C. Case of a general (nonfactorized) RS solution

In a general case when the replica symmetric solution is not factorized, e.g., in the canonical case of the random K-SAT problem, the situation is a bit more complex. In the gendanken experiment of Sec. III A, the uniform boundary conditions have been created with (and thus depends on) the replica symmetric marginals $\bar{\psi}$. The procedure described in the gedanken experiment translates to a more general form of equations that are exact on a tree. The equivalent of Eq. (24) then reads

$$\bar{\psi}_s \bar{P}_s(\psi|\bar{\psi}) \mathcal{P}_{\mathrm{RS}}(\bar{\psi}) = \sum_J Q(J) \sum_{\{l\}} q(\{l\}) \int \prod_{i=1}^{K-1} \prod_{j=1}^{l_i} \times [d\bar{\psi}^j \mathcal{P}_{\mathrm{RS}}(\bar{\psi}^j)] \delta[\bar{\psi} - \mathcal{F}(\{\bar{\psi}^j\}, \beta_e)] \times \sum_{\{s_i\}} e^{\beta_e C(J,s,\{s_i\})} \frac{\prod_{i=1}^{K-1} \prod_{j=1}^{l_i} \bar{\psi}_{s_i}^j}{Z(\{\bar{\psi}^j\}, \beta_e)} \int \prod_{i=1}^{K-1} \prod_{j=1}^{l_i} \times [d\psi^j \bar{P}_{s_i}^j(\psi^j|\bar{\psi}^j)] \delta[\psi - \mathcal{F}(\{\psi^j\}, \beta_a)], \quad (27)$$

where $C(J,s,\{s_i\})$ is an arbitrary interaction between spins $s,\{s_i\}$ of strength J, in case of XOR-SAT we had $C(J,s,\{s_i\}) = J\beta_e s \Pi_i s_i$. This equation is maybe easier to understand from the population dynamics procedure used to solve it. Now we have $|s|+1$ different arrays to represent the messages. In the first array we initially put an equilibrated replica symmetric population (values obtained by solving the simple RS equations by population dynamics). In the array corresponding to value s we initially put a message completely polarized in the direction s.

Updating one element has to be done in all the $|s|+1$ arrays simultaneously. One first chooses the degrees l_i, then one chooses the corresponding number of random elements in the population. One uses the first array to compute the new value corresponding to the first array in the new element. To compute a new value corresponding to array s one uses the values on the first array to draw a configuration of values $\{s_i\}$ using probabilities,

$$P(\{s_i\}|\{\bar{\psi}^j\}, \beta_e, s) = e^{\beta_e C(J,s,\{s_i\})} \frac{\prod_{i=1}^{K-1} \prod_{j=1}^{l_i} \bar{\psi}_{s_i}^j}{Z(\{\bar{\psi}^j\}, \beta_e)}. \quad (28)$$

Finally using elements in arrays corresponding to values s_i one computes a new value. This done for every value of s finalizes one step. All is repeated until convergence is reached. The expression for the free energy is analogous to Eq. (26) using the same generalization as for Eq. (27).

We note that when $\beta_e = \beta_a$, the above equations are actually already known, and are exactly equivalent to the 1RSB equations at $x=1$. Again, this is just because in that case, we are simply describing the properties of a typical state. With equal temperatures, the above form of the 1RSB equations at $x=1$ appeared in Refs. 48, 50, and 51 (to which we refer the reader interested to see how the present derivation generalizes) and similar equations appeared in the context of the analysis of an idealized BP decimation algorithm in Refs. 52 and 53.

D. Relation to the problem of reconstruction on trees

In the special case when $T_e = T_a$ the above equations are thus equivalent to the 1RSB equations when the Parisi pa-

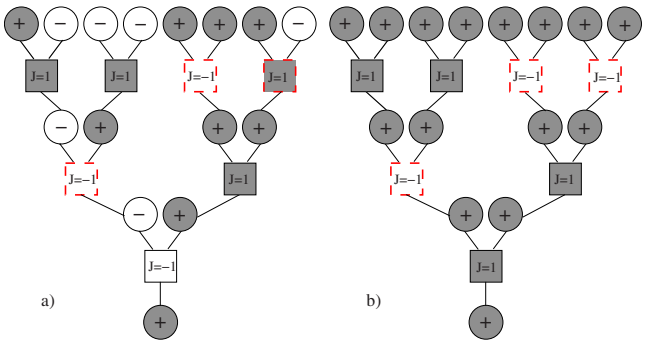

FIG. 3. (Color online) (a) Recursive construction of an equilibrium configuration at temperature T_e in XOR-SAT. Given the tree, and a random choice of interactions (full square $J=1$, empty square $J=-1$), one starts from the root, and chooses iteratively the configuration of the ancestors (full circles $s=1$, empty circle $s=-1$) randomly such that it satisfies the constraints with probability $1-\epsilon(T_e)$, Eq. (15), here $\epsilon=3/7$. Violated constraints have dashed/red borders. (b) The problem can also be gauge transformed using Eq. (29), see Sec. III F, into a fully polarized configuration with all $s=1$ but where the J's are chosen from distribution, Eq. (30).

rameter $x=1$, and are closely related to the problem of reconstruction of trees, an important setting in computer science and information theory, as was realized by Mézard and Montanari.[26] In the reconstruction on trees, a single configuration is spread from the root of the tree to its leaves with some given rules and noise level, and the task is then to reconstruct (infer) the value of the root based on the configuration on the leaves. In particular, in a model with a factorized replica symmetric solution, constructing an equilibrium configuration on the tree has a simple local interpretation, as, e.g., in Ref. 26. The noise level corresponds to the equilibrium temperature T_e. This spreading construction is *precisely* the one we have used in Fig. 3 for the XOR-SAT problem: starting from a value of the spin chosen randomly, we have chosen iteratively the configuration of the other variables randomly such that it violates the constraints with probability ϵ corresponding to T_e.

In the reconstructing on trees one thus applies BP starting from the leaves, using the values on the boundaries as starting conditions, to generate the marginal distributions of the variables within the tree. This is precisely what we have done, the only difference is that in the reconstruction formalism, one *knows* the value of ϵ that has been used in order to construct the configuration on the tree, and therefore, one used the same value in the BP equation in the recovery process. The states following problem is thus a generalization of the reconstruction on trees, where one first generates the configuration with a value ϵ_e (corresponding to a temperature T_e) but then apply the BP equation with a different value ϵ_a (corresponding to a temperature T_a).

1. Reconstruction in a noisy channel without knowledge of the noise

The method of states following can thus be viewed as a variant of reconstruction on trees. In this interpretation the noise of the channel is described by the inverse temperature β_e. If this value is unknown, the task of reconstructing the values will be done with *a priori* different temperature β_a: the behavior of Eq. (24) thus describes the reconstruction problem where the noise level of the channel is not known.

Two interesting remarks can be done at this point. First, it follows from the maximum likelihood principle that the best chance to reconstruct corresponds to $\beta_e=\beta_a$, and in fact, this gives a direct way to recover the noise value by maximizing the free energy. On a tree, both the noise value and the marginal distribution can thus be recovered in the reconstruction process. A second point is that, as we will see from the behavior of the states following method, in some cases although reconstruction is possible at $\beta_a=\beta_e$ it might *not* be possible at some $\beta_a>\beta_e$ (that is when trying to reconstruct by assuming the number of mistake *smaller* than the actual value), which is rather counterintuitive.

2. Better bound for noisy reconstruction

A last point we shall mention is that our method provides a simple way to have better bounds on noisy reconstruction. Consider indeed a problem where we have generated the boundaries with a noise level β_e. We now use a very simple algorithm: we do the BP recursion with $\beta_a\to\infty$, that is, assuming that no mistakes were done in the process. In that case, a simple bound of the reconstruction threshold can be obtained by considering a probability when the boundary condition directly imply the correct value of the root.[49,54] A similar procedure for $T_e=0$ was called *naive reconstruction* in Refs. 49 and 50.

In the case $\beta_a\to\infty$ the equations simplify and can be cast in a set of coupled equations with two variables—one being the probability that the value of the root is implied in the actual value, second being the probability that the value is implied wrongly. As long as the first probability is larger than the second, which is always the case in the cases we studies, this leads to better bounds on the noisy reconstruction problem. Some of these values are given in Sec. VI C for the XOR-SAT problem. In fact, it is simply the generalization of the *naive reconstruction* bound to the case of noisy channels.[49,54]

E. Quiet planting: How to simulate impossible to simulate models?

The construction we have described is related to the notion of quiet planting, which turns out to be a powerful way to perform simulations for the mean-field models that would not be possible otherwise. Let us first stress that the thought experiment of choosing an equilibrium configuration, that lead us to the derivation on above equations, is feasible *only* on trees. On a random graph we would encounter problems as soon as the long cycles start appearing when proceeding from a node playing the role of the root. Indeed, choosing an equilibrium configuration on a given random graph below the dynamical temperature T_d requires, as far as we know, an exponential time.

This difficulty, however, can be bypassed in the special cases where the replica symmetric solution is factorized and in this case the adiabatic evolution of states is realizable also

on single graph instances. This has interesting algorithmic applications: it is possible to create a graph *and* an equilibrated configuration at the same time. The point is that when the RS solution is factorized it is possible to create a typical random graph (from the ensemble under consideration) and a configuration that is an equilibrium configuration at temperature $T_e \geq T_K$ on that graph. This concept was called *quiet planting* and was discussed by the authors in Refs. 47 and 48.

Let us first define quiet planting in the XOR-SAT problem and then justify the above-claimed properties. Planting an equilibrium configuration in XOR-SAT at a given temperature (or equivalently at a given energy) works as follows: first choose a random configuration of spins $\{\sigma_i\}$, then choose a random instance from the ensemble under consideration restricted to the fact that $(1-\epsilon)M$ constraints are satisfied by the chosen configuration of spins and ϵM are not satisfied. Thus, given the configuration, choose at random ϵM [$(1-\epsilon)M$, respectively] constraints out of all the possible satisfied (unsatisfied, respectively) constraints. The fraction ϵ is a function of the temperature β_e, and it is given by Eq. (15). This way for one given clause, out of the 2^{K-1} configuration that do not satisfy that clause, each will happen with probability $\epsilon/2^{K-1}$, each satisfying configurations will appear with probability $(1-\epsilon)/2^{K-1}$. If we condition on the value of one variable contained in the clause we obtain probabilities in Eq. (23). Thus if we look on a finite neighborhood of a variable in a very large planted hypergraph we will obtain a hypertree statistically identical to the one described in Sec. III A. Consequently, Eqs. (24) and (26) are the cavity equations describing the properties of the planted graph. As typical properties of the graph follow from the solution of Eq. (24), the planted graph and the planted configuration will have the same typical properties as a random graph and an equilibrium configuration. Hence, justification of the name *quiet* planting, i.e., planting that does not change typical properties of the ensemble.

Note here that the above argument was possible only because the probabilities in Eq. (23) were independent of the values of messages $\{\psi^{b\to j}\}$. On the other hand, whenever this is the case, i.e., whenever the replica solution is factorized, the above argument is valid. In a general factorized case, i.e., for nonsymmetric interactions or when disorder in the interactions is present, the planting procedure have to be slightly generalized. The marginal probabilities are used to plant a configuration with a proper number of each value (proper magnetization). Based on the RS solution one has to compute probabilities that a given type of constraint has a given set of values on its neighboring variables and plant the constraints accordingly. An example of this generic procedure at zero temperature was described in detail in Ref. 48.

It shall be noted at this point that the equivalence between the planted and purely random ensemble has been proven rigorously in Ref. 55 in the zero-temperature case in the region of parameters where the second moment of the number of solutions is smaller than some constant times the square of the first moment. E.g., in the coloring problem for three colors the above holds till average degree $c_q(3)=3.83$, for four colors until $c_q(4)=7.81$, to be compared with the Kauzmann transition, also called the condensation transition, $c_c(3)=4$ and $c_c(4)=8.46$. In the factorized models the annealed free energy, $\log\langle Z\rangle$, starts to differ from the quenched one $\langle \log Z\rangle$ at the Kauzmann transition,[41] and then the equivalence between the two ensembles breaks down.

Even before the proofs of[55] the equivalence between the planted and random ensemble for XOR-SAT for connectivities below the condensation transition was proven in,[21] Appendix A. In this special case the equality of the annealed and quenched free energies is directly linked to the absence of hyperloops in the graph.[21] Authors of Ref. 21 used the equivalence between the planted and random ensembles and the fact that the planted configuration is one of the equilibrium configurations as a handy tool to equilibrate their Monte Carlo simulations even at temperatures where the usual equilibration is impossible in feasible times.

The possibility of generating, *for free,* an equilibrium configuration together with a typical realization of the disorder for all temperatures $T>T_K$ is extremely useful and allows to perform simulations that would be impossible otherwise. Indeed for all the range of temperatures $T_K \leq T \leq T_d$, it is unfeasible to find an equilibrium configuration as soon as N is not ridiculously small. With the quiet planting method, this limitation disappears. The present authors have already used this in Refs. 47 and 48, where one benefited from the fact that Monte Carlo, belief propagation, and other dynamical procedures can be initialized in a truly equilibrium configuration. Later on, in Sec. VI, we will use this trick of quiet planting to confirm numerically, through Monte Carlo simulations and the use of BP equations, the results of the states following method.

F. Reformulation using mapping on the Nishimori line

A last, and maybe most striking, relation to previous works arises when one considers gauge transformations. Let us consider, again, the p-spin model. The equations for adiabatic evolution of states can be further simplified by exploiting a gauge invariance. Indeed for any spin i, the transformation

$$s_i \to -s_i \quad \text{and} \quad J_a \to -J_a \quad \forall\, a \in \partial i \tag{29}$$

keeps Hamiltonian (1) invariant. As shown in Fig. 3, this allows to transform the equilibrium spin configuration on any graph into a uniform one (all $s=1$), the disorder distribution then changes from Eq. (2) with $\rho=1/2$ to

$$Q_{\mathrm{NL}}(J) = \epsilon(T_e)\,\delta(J+1) + [1-\epsilon(T_e)]\,\delta(J-1), \tag{30}$$

where $\epsilon(T_e)$ is given by Eq. (15). Since all $s=1$, there is no need to distinguish between the +1 and the −1 sites. Equation (24) reduces to the usual replica symmetric cavity equation for a problem with mixed ferromagnetic/antiferromagnetic interactions at temperature T_a initialized in the uniformly positive state

$$P_s(\psi) = \sum Q_{\mathrm{NL}}(J) \sum_{\{l_i\}} q(\{l_i\}) \int \prod_{i=1}^{K-1} \prod_{j=1}^{l_i} dP(\psi^j)\, \delta[\psi - \mathcal{F}(\{\psi^j\}, \beta_a)], \quad P_{\mathrm{init}}(\psi) = \delta\left[\begin{pmatrix} \psi_1 \\ \psi_0 \end{pmatrix} - \begin{pmatrix} 1 \\ 0 \end{pmatrix} \right]. \tag{31}$$

The distribution of interactions, Eq. (30), is given by the Nishimori-type[29,56] relation between temperature T_e and density of antiferromagnetic couplings ϵ, and arises because at $T_a = T_e$ the overlap with the equilibrium configuration, playing a role of magnetization m in the gauge-transformed model, is equal to the overlap q between two typical configurations from the state, a well-known property of the so-called Nishimori line (that is the line defined by the Nishimori relation in the temperature/ferromagnetic bias plane).

The gauge invariance has thus transformed the task of following an equilibrium state in a glassy model into describing the evolution of the ferromagnetic state in a ferromagnetically biased model with the standard cavity approach. As we will derive in Sec. V B the adiabatic evolution of states in the fully connected p-spin model for $T_e \geq T_K$ is thus equivalent to solving the p-spin model with an additional effective ferromagnetic coupling Eq. (52), and one can thus readily take the solution of the p spin in the literature, e.g., Refs. 56 and 57 to obtain properties of the equilibrium states.

A similar mapping exists for all mean-field models where the replica symmetric solution is factorized (see, for instance, Ref. 58 for glassy Potts models), however, the resulting model is not always very natural nor already known. For the p-spin model the evolution of a glassy state being equivalent to melting of the ferromagnetic state on the Nishimori line has deep consequences for the physics of glasses, as will be discussed elsewhere.[59]

IV. EVOLUTION OF STATES: GENERAL CAVITY EQUATIONS FOR ANY TEMPERATURE

In this section we introduce a method of states following that is suitable at any temperature and where replica symmetry breaking is thus taken into account. The method is set for any 1RSB states, at any value of the Parisi parameter x and any temperature, as long as the corresponding states are stable toward further steps of replica symmetry breaking. Stability of the following equations toward RSB for different values of β_a is interesting and will be discussed later.

A. Adiabatic evolution of 1RSB states

In order to understand the general equations for the adiabatic evolution of states, let us first briefly recall how are derived the cavity 1RSB equations that describe the equilibrium states. We work at inverse temperature β_e where many states exist, each of them has a corresponding BP fixed point, i.e., a message ψ on each link. As described in Sec. II A 2, the 1RSB method uses the distribution of messages $P(\psi, \beta_e)$ over all states with a given free energy f. In order to select the free energy, we consider the BP recursion in every possible state but we reweight each state according to $Z^x(\psi, \beta_e)$. This leads to Eq. (16).

One intuitive way to understand Eq. (16) is to think about the problem on a tree and consider many possible boundary conditions $P_{\mathrm{init}}(\psi, \beta_e)$. In order to select boundary conditions that lead to the state of free energy f we reweight $P(\psi, \beta_e)$ at each steps with $Z^x(\psi, \beta_e)$. Eventually, for different x such fixed point will describe states with different free energy f. For more details on this derivation see Refs. 17, 50, and 51.

In order to write the equations for the adiabatic evolution of the 1RSB states, we first need to describe the state via Eq. (16), and second we use another distribution $\tilde{P}(\psi, \tilde{\psi})$ that describes the same state at a new temperature β_a. The equilibrium states at temperature β_e arise if one uses the reweigthing $Z^x(\psi, \beta_e)$. The probability distribution $\tilde{P}(\psi, \tilde{\psi})$ thus needs to be reweighted with the same factor $Z^x(\psi, \beta_e)$ in the state following method. Thus, the generalization of the 1RSB equations to the state following is a recursion on both $P(\psi)$ and $\tilde{P}(\psi, \tilde{\psi})$ as follows:

$$\begin{aligned} \tilde{P}^{a\to i}(\psi^{a\to i}, \tilde{\psi}^{a\to i}) = \frac{1}{\mathcal{Z}^{a\to i}(\beta_e, \beta_a)} \int \prod_{j\in\partial a\backslash i} \prod_{b\in\partial j\backslash a} & \times d\tilde{P}^{b\to j}(\psi^{b\to j}, \tilde{\psi}^{b\to j}) \\ & \times [Z^{a\to i}(\{\psi^{b\to j}\}, \beta_e)]^x \delta[\psi^{a\to i} \\ & - \mathcal{F}(\{\psi^{b\to j}\}, \beta_e)] \delta[\tilde{\psi}^{a\to i} - \mathcal{F}(\{\tilde{\psi}^{b\to j}\}, \beta_a)]. \end{aligned} \tag{32}$$

The distribution $\tilde{P}$ is initialized as

$$\tilde{P}^{a\to i}(\psi^{a\to i}, \tilde{\psi}^{a\to i}) = P^{a\to i}(\psi^{a\to i})\, \delta(\psi^{a\to i} - \tilde{\psi}^{a\to i}), \tag{33}$$

where the $P^{a\to i}(\psi^{a\to i})$ is the solution of the usual 1RSB Eq. (16) describing the equilibrium state at an inverse temperature β_e. Equation (32) then describes adiabatic evolution of this state at an inverse temperature β_a. Note that the reweighting factor Z^x comes from the messages ψ as the inverse temperature β_e—again, this is the key element assuring that we are looking into the same state at a different temperature.

The internal free energy of the state at temperature β_a is given in terms of node and link contributions, as usual in the 1RSB cavity method,

$$-\beta_a F(\beta_a) = -\beta_a \sum_a F^{a+\partial a}(\beta_a) + \beta_a \sum_i (l_i - 1) F^i(\beta_a), \tag{34}$$

where

$$-\beta_a F^{a+\partial a}(\beta_a) = \frac{\int \prod_{i\in\partial a}\prod_{b\in\partial i\backslash a} d\tilde{P}^{b\to i}(\psi^{b\to i},\tilde{\psi}^{b\to i})[\log Z^{a+\partial a}(\{\tilde{\psi}^{b\to i}\},\beta_a)][Z^{a+\partial a}(\{\psi^{b\to i}\},\beta_e)]^x}{\int \prod_{i\in\partial a}\prod_{b\in\partial i\backslash a} d\tilde{P}^{b\to i}(\psi^{b\to i},\tilde{\psi}^{b\to i})[Z^{a+\partial a}(\{\psi^{b\to i}\},\beta_e)]^x}, \tag{35}$$

$$-\beta_a F^{i}(\beta_a) = \frac{\int \prod_{a\in\partial i} d\tilde{P}^{a\to i}(\psi^{a\to i},\tilde{\psi}^{a\to i})[\log Z^{i}(\{\tilde{\psi}^{a\to i}\},\beta_a)][Z^{i}(\{\psi^{a\to i}\},\beta_e)]^x}{\int \prod_{a\in\partial i} d\tilde{P}^{a\to i}(\psi^{a\to i},\tilde{\psi}^{a\to i})[Z^{i}(\{\psi^{a\to i}\},\beta_e)]^x}. \tag{36}$$

And for the corresponding energy we have

$$E(\beta_a) = \sum_a \frac{\int \prod_{i\in\partial a}\prod_{b\in\partial i\backslash a} d\tilde{P}^{b\to i}(\psi^{b\to i},\tilde{\psi}^{b\to i})E^{a+\partial a}(\{\tilde{\psi}^{b\to i}\},\beta_a)[Z^{a+\partial a}(\{\psi^{b\to i}\},\beta_e)]^x}{\int \prod_{i\in\partial a}\prod_{b\in\partial i\backslash a} d\tilde{P}^{b\to i}(\psi^{b\to i},\tilde{\psi}^{b\to i})[Z^{a+\partial a}(\{\psi^{b\to i}\},\beta_e)]^x}. \tag{37}$$

Equations (32)–(37) are written for a given instance of the problem. It is instructive to describe how to solve them on average over the graph ensemble using the population dynamics method.[19] We need to keep a population (representing the distribution over the graph edges) of couples of messages (one for ψ, the other for $\tilde{\psi}$). Then the population is iterated in the exact same way as in the usual case,[19] the whole population of couples is reweighted using the reweighting factor $[Z^{a+\partial a}(\{\psi^{b\to i}\},\beta_e)]^x$ computed from the elements ψ at inverse temperature β_e.

B. When states themselves divide into states

So far, we supposed that the state we are following does not exhibit an instability toward replica symmetry breaking. This assumption may break when temperature T_a is low enough. To check for the local stability we can use a variant of any known method, see, e.g., Ref. 60 or Appendix C of Ref. 50. One of the methods, simplest to implement in the population dynamics, is the monitoring of deviation of two replicas. For that we first need to find an equilibrated population at a temperature T_a, then we copy this population and introduce a small noise. Further the two copies (replicas) are updated with the same random choices and the deviation of the two is monitored. If the deviation is going to zero the state is locally stable, if the deviation is growing the state is not stable toward replica symmetry breaking that is the state has the tendency to divide into many smaller states. This second case can be treated in the following way.

If the state to be followed is not stable toward replica symmetry breaking then applying the 1RSB method within this state shall lead better result about its behavior. The following equations together with Eqs. (16) and (32) describes the method

$$P_2^{a\to i}(\tilde{P}^{a\to i}) = \frac{1}{\mathcal{Z}_2^{a\to i}}\int \prod_{j\in\partial a\backslash i}\prod_{b\in\partial j\backslash a} dP_2^{b\to j}(\tilde{P}^{b\to j}) \times [\mathcal{Z}^{a\to i}(\beta_e,\beta_a)]^{x_2}\delta[\tilde{P}^{a\to i} - \mathcal{F}_2(\{\tilde{P}^{b\to j}\},\beta_e,\beta_a)], \tag{38}$$

where the functional $\mathcal{F}_2(\{\tilde{P}^{b\to j}\},\beta_e,\beta_a)$ is defines by Eq. (32). Said in words, on every edge next to the population corresponding to Eq. (16) one would have to keep a population of populations, each corresponding to a substrate. Each of these populations would be reweighted using the reweighting from Eq. (16). A second reweighting with Parisi parameter x_2 would have to be done on the level of populations. On top of all that in the nonfactorized cases a population of these object would have to be kept to account for the average over the graph. Numerical resolution of such equations becomes involved and we let their implementation for the diluted models for future works.

V. FIRST APPLICATION: ADIABATIC EVOLUTION OF STATES IN THE FULLY CONNECTED *p*-SPIN MODEL

Now that we have presented the method for adiabatic evolution of states, let us show how does the solution of the equations behave and what can be learned about the physics of the p-spin problem. We will also describe here the connection of the states following method to the Franz-Parisi potential[27,28] and with the physics on the Nishimori line.

One of the simplest cases to which Eq. (24) can be applied is the fully connected p-spin model. The static replica solution of the model is in Ref. 37. In Appendix A we show how to rederive the replica symmetric equations for the fully connected p-spin model as a limit of infinite connectivity of the cavity (belief propagation) equations (24). Here we only

summarize the equations needed to explain how to obtain the solution for state following.

A. Equilibrium solution of the fully connected *p*-spin model

As discussed in details in Appendix A, BP simplifies in the fully connected model where the amplitudes of all interactions are small, and become

$$m^{i\to a} = \tanh\left(\beta \sum_{b\in\partial i\backslash a} J_b \prod_{j\in\partial b\backslash i} m^{j\to b}\right), \tag{39}$$

where m the local cavity magnetization. The replica symmetric solution can then be written in terms of the distribution of such cavity magnetization that are Gaussian because of the central limit theorem:[61,62] we thus need only the average magnetization $m=\langle m^{i\to a}\rangle$ and the average overlap between configuration $q=\langle (m^{i\to a})^2\rangle$. The recursion reads

$$m = \int_{-\infty}^{\infty} \mathcal{D}y \tanh(\beta J y\sqrt{pq^{p-1}/2} + \beta J_0 p m^{p-1}), \tag{40}$$

$$q = \int_{-\infty}^{\infty} \mathcal{D}y \tanh^2(\beta J y\sqrt{pq^{p-1}/2} + \beta J_0 p m^{p-1}), \tag{41}$$

where we call $\mathcal{D}y=dye^{-y^2/2}/\sqrt{2\pi}$ the Gaussian integration. The free energy is a function of the fixed point of the above equations,

$$\begin{aligned} -\beta f = {} & \frac{1}{4}\beta^2 J^2 (p-1) q^p - \beta J_0 (p-1) m^p + \frac{1}{4}\beta^2 J^2 \\ & - \frac{1}{4}\beta^2 J^2 p q^{p-1} + \int \mathcal{D}y \log 2\cosh(\beta J y\sqrt{pq^{p-1}/2} \\ & + \beta J_0 p m^{p-1}) \end{aligned} \tag{42}$$

and for the replica symmetric energy density we have

$$e = \frac{\partial(\beta f)}{\partial\beta} = -J_0 m^p - \frac{1}{2}\beta J^2 (1-q^p). \tag{43}$$

The 1RSB solution with the value of Parisi parameter x is obtained in a similar way and the corresponding fixed-point equations are

$$m = \int \mathcal{D}u \left[\frac{\int \mathcal{D}v \cosh^x(\beta G)\tanh(\beta G)}{\int \mathcal{D}v \cosh^x(\beta G)} \right], \tag{44}$$

$$q_1 = \int \mathcal{D}u \left[\frac{\int \mathcal{D}v \cosh^x(\beta G)\tanh^2(\beta G)}{\int \mathcal{D}v \cosh^x(\beta G)} \right], \tag{45}$$

$$q_0 = \int \mathcal{D}u \left[\frac{\int \mathcal{D}v \cosh^x(\beta G)\tanh(\beta G)}{\int \mathcal{D}v \cosh^x(\beta G)} \right]^2, \tag{46}$$

where

$$G = Ju\sqrt{\frac{p}{2}q_0^{p-1}} + Jv\sqrt{\frac{p}{2}q_1^{p-1} - \frac{p}{2}q_0^{p-1}} + J_0 p m^{p-1} \tag{47}$$

is a sum of two Gaussian variables and $\mathcal{D}$ is the Gaussian integral. The parameter q_1 is the average self-overlap and q_0 the average overlap between states. The 1RSB Parisi (replicated) free energy reads

$$\begin{aligned} -\beta x\Phi(\beta,x) = {} & -x\beta J_0 p m^p + \frac{1}{4}(1-x)x(p-1)\beta^2 J^2 q_1^p \\ & + \frac{1}{4}x^2(p-1)\beta^2 J^2 q_0^p + \frac{1}{4}\beta^2 J^2 x - \frac{1}{4}\beta^2 J^2 x p q_1^{p-1} \\ & + x\log 2 + \int \mathcal{D}u \log \int \mathcal{D}v \cosh^x \beta G, \end{aligned} \tag{48}$$

the free energy is derived as $f(\beta)=\partial\Phi(\beta,x)/\partial x$.

B. Equations for adiabatic evolution of states for $T_e \geq T_K$

Let us give a derivation of state following equations for the fully connected p-spin model using the equivalence with the planted ensemble. We think about the fully connected model as the large connectivity version of the diluted model and use the planting procedure described in Sec. III E. We first plant an equilibrium configuration at inverse temperature β_e, then initialize the belief propagation equations in this configuration and iterate to a fixed point at another inverse temperature β_a. When the temperature of planting is larger than the Kauzmann temperature, $\beta_e<\beta_K$, then the planting can be done in a very natural way. One first takes the replica symmetric energy at β_e and computes the corresponding fraction ϵ of interactions that are not satisfied at that energy. Then when constructing the planted graph one first chooses a random configuration, the sign of interactions is then chosen in such a way that fraction ϵ of them is unsatisfied and $1-\epsilon$ satisfied.

The value of ϵ in the fully connected p-spin model is computed as follows. Let us assume $J_0=0$, as this is really the case we are interested in, recall that we rescale the interactions in the fully connected model as $\langle J_a^2\rangle = J^2 p!/(2N^{p-1})$, hence $J_a=\pm J\sqrt{p!/(2N^{p-1})}$, there is total of $N^p/p!$ interactions. The energy we want to achieve is given by Eq. (43), hence ϵ has to satisfy

$$\epsilon = \frac{1}{2} - \beta_e \frac{J(1-q^p)}{2}\sqrt{\frac{p!}{2N^{p-1}}}. \tag{49}$$

Moreover as we consider only $\beta_e<\beta_K$, in the p-spin model this means that $q=0$.

Now let us keep in mind the above planting, moreover consider that spin i was planted +1 (without loss of generality) and look back at Eq. (39), considering $J_0=0$. The terms

in the sum in the argument of the tanh are independent (by the assumption of replica symmetry within the planted state) and their statistics is thus ruled by the central limit theorem. Thus our aim is to compute the mean and variance of the argument. If the interactions would not be correlated with the planted configuration the mean would be zero (remind we have $J_0=0$). If we satisfy every interaction with probability $1-\epsilon$, there will be $1-2\epsilon$ more satisfied interactions than unsatisfied ones. These $1-2\epsilon=2\beta_e J\sqrt{p!/8}/N^{(p-1)/2}$ interactions are biasing spin i in the direction +1. The mean of the argument of the tanh is thus

$$\mu = \beta_a \frac{N^{p-1}}{(p-1)!}\frac{2\beta_e J\sqrt{p!/8}}{N^{(p-1)/2}}\sqrt{\frac{J^2 p!}{2N^{p-1}}}m^{p-1}$$

$$= \beta_a\beta_e J\sqrt{p!/8}J\frac{\sqrt{2p!}}{(p-1)!}m^{p-1} = \beta_a[\beta_e J^2/2]pm^{p-1}. \quad (50)$$

The planting only influences the directions of the interactions, thus in the variance computation nothing changes and we have again

$$\sigma = \beta_a^2 J^2 p q^{p-1}/2. \quad (51)$$

Thus parameters $m=\langle m^{i\to a}\rangle$ and $q=\langle (m^{i\to a})^2\rangle$ are ruled again by Eqs. (40) and (41) with inverse temperature β_a and effective coupling

$$J_0^{\mathrm{eff}} = \beta_e J^2/2. \quad (52)$$

Parameter m now measures how far from the equilibrium planted configuration is a typical configuration at β_a. Also the free energy Eq. (42) applies to this case with inverse temperature β_a and effective J_0^{eff} given by Eq. (52). The free energy here is, however, free energy of the planted state and thus the complexity, defined by Eq. (17) with $x=1$, can be computed considering the difference

$$\Sigma = -\beta_a f(J_0=0) + \beta_a f(J_0^{\mathrm{eff}}). \quad (53)$$

Consequently all the physics of adiabatic evolution of states above the Kauzmann temperature for the $J_0=0$ model can be induced from the known phase diagram of the $J_0\neq 0$ model and Eq. (52) is the Nishimori line condition[29,56] for the fully connected p-spin model with a nonzero J_0. This illustrates the general equivalence we have discussed in Sec. III F between the states following method and the original model on the Nishimori line.

The dynamical temperature can be interpreted as the spinodal point of the planted state, thus if $\beta_e=\beta_a$ we start to have a nontrivial solution at T_d. And at T_K the complexity, Eq. (53), becomes negative. Iterating Eqs. (40) and (41) we indeed obtain values of the two critical temperatures as known from the 1RSB solution of the p-spin model. For $p=3$ we have $T_K=0.6513$ and $T_d=0.6815$.

In the case of the fully connected p-spin model the state following when states start to be unstable (divide into substates), described in generality in Sec. IV B, can be done easily (at least on the 1RSB level) by using the mapping on a model with effective ferromagnetic coupling. Again, for the model with $J_0=0$ the 1RSB solution inside a state is equivalent to the standard 1RSB solution in a model with $J_0^{\mathrm{eff}}=\beta_e J^2/2$, Eqs. (44)–(46).

C. Equations for adiabatic evolution of states for $T_e<T_K$

We now want to follow states below the Kauzmann temperature, or metastable states above T_K (i.e., at a Parisi parameter $x\neq 1$). As far as we know there is no *planting* interpretation for this case, the mapping into ferromagnetically biased model on the Nishimori line does not work either in this case. The underlying equilibrium measure at $T_e<T_K$ becomes more complicated, the derivation then must follow by rewriting Eqs. (16) and (32) in the large connectivity limit.

For simplification we note that in the p-spin model with $J_0=0$ we have $m=q_0=0$ thus the only nontrivial parameter describing the 1RSB state we aim to follow is q_1, given by the Eq. (45), this summarizes Eq. (16).

To rewrite Eq. (32) we need to introduce overlap $\tilde{q}_1$ and a correlation between the two populations

$$\tilde{q}_1 = \int \mathcal{D}Q(P)\left[\frac{\int d\tilde{P}(m^{i\to a},\tilde{m}^{i\to a})Z(\{m^{i\to a}\},\beta_e)^x(\tilde{m}^{i\to a})^2}{\int dP(m^{i\to a})Z(\{m^{i\to a}\},\beta_e)^x}\right]$$

$$\equiv \langle\langle(\tilde{m}^{i\to a})^2\rangle_{\tilde{P},P}\rangle_Q, \quad (54)$$

$$c = \int \mathcal{D}Q(P)\left[\frac{\int d\tilde{P}(m^{i\to a},\tilde{m}^{i\to a})Z(\{m^{i\to a}\},\beta_e)^x m^{i\to a}\tilde{m}^{i\to a}}{\int dP(m^{i\to a})Z(\{m^{i\to a}\},\beta_e)^x}\right]$$

$$\equiv \langle\langle m^{i\to a}\tilde{m}^{i\to a}\rangle_{\tilde{P},P}\rangle_Q. \quad (55)$$

In Appendix A 3 we remind the derivation of the standard 1RSB equations for the fully connected p-spin model. What we need here goes in a very similar manner. We define

$$X = \sum_{b\in\partial i\backslash a} J_b \prod_{j\in\partial b\backslash i} m^{j\to b}, \quad \tilde{X} = \sum_{b\in\partial i\backslash a} J_b \prod_{j\in\partial b\backslash i} \tilde{m}^{j\to b} \quad (56)$$

and obtain similarly as in Appendix A 3,

$$\sigma_1^2 = \langle\langle X^2\rangle_{P,\tilde{P}}\rangle_Q = J^2\frac{p}{2}q_1^{p-1}, \quad (57)$$

$$\tilde{\sigma}_1^2 = \langle\langle \tilde{X}^2\rangle_{P,\tilde{P}}\rangle_Q = J^2\frac{p}{2}\tilde{q}_1^{p-1}, \quad (58)$$

$$\rho = \frac{\langle\langle X\tilde{X}\rangle_{P,\tilde{P}}\rangle_Q}{\sigma_1\tilde{\sigma}_1} = \left(\frac{c}{\sqrt{q_1\tilde{q}_1}}\right)^{p-1}. \quad (59)$$

The final self-consistent equations for $\tilde{q}_1$ and c are then

$$\tilde{q}_1 = \frac{\int \mathcal{D}\{u,v\}\cosh^x(\beta_e v)\tanh^2(\beta_a u)}{\int \mathcal{D}v\,\cosh^x(\beta_e v)}, \quad (60)$$

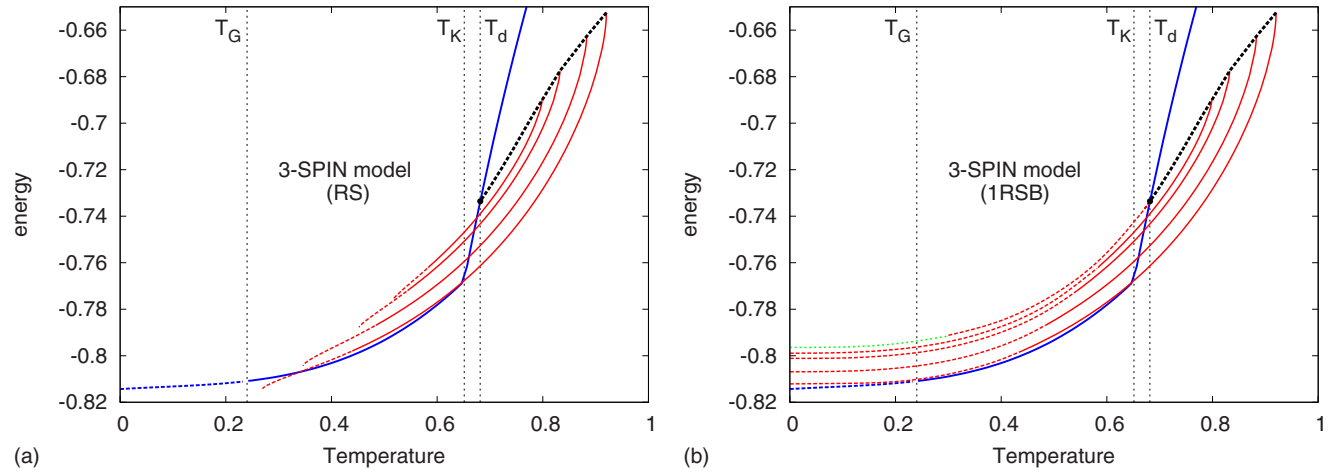

FIG. 4. (Color online) Adiabatic evolution of states in the fully connected three-spin model, where T_d=0.6815 and T_K=0.6513. The continuous (blue) curve that crosses the graph shows the equilibrium energy $e_e(T)$ of the model versus the temperature (with the Gardner transition toward full RSB phase at low temperature). We have applied the states following method and the red curves (five roughly parallel curves) mark the adiabatic evolution of states from equilibrium with T_e=0.6815,0.675,0.67,0.66,0.6513 for temperatures $T_a \neq T_e$. Left: this is the RS result where we follow states using the RS ansatz, Eqs. (40), (41), and (43). Upon warming, the states exist until meeting a spinodal point at much larger temperature. Upon cooling the states can be followed until they become unstable against 1RSB (dashed), eventually a nonphysical spinodal point makes the RS solution vanish. Note that the RS solution for the equilibrium state at $T_e=T_d$ vanishes as soon as $T_a<T_e$ and is thus not even seen on this picture. Right: we follow states using the 1RSB ansatz (the dashed part of the red curves), Eqs. (44)–(48). The 1RSB solution is actually also unstable to further steps of RSB and (most probably) the full RSB should be used instead. The 1RSB is therefore a (good) lower bound to the correct result. Note also that the nonphysical spinodal points for low temperatures do not appear and that the 1RSB approach has mostly cured the problem with the exception of the states corresponding to $T_e \approx T_d$. The green dotted line is an example of a region where even the 1RSB equations do not have a physical solution. The green dotted line is a lower bound computed by the construction suggested in Sec. V G 2.

$$c = \frac{\int \mathcal{D}\{u,v\}\cosh^x(\beta_e v)\tanh(\beta_e v)\tanh(\beta_a u)}{\int \mathcal{D}v\ \cosh^x(\beta_e v)}, \tag{61}$$

where

$$\mathcal{D}\{u,v\} = \frac{1}{2\pi\sigma_1\tilde{\sigma}_1\sqrt{1-\rho^2}}\exp\left[-\frac{1}{2(1-\rho^2)}\left(\frac{u^2}{\tilde{\sigma}_1^2}+\frac{v^2}{\sigma_1^2} - \frac{2\rho uv}{\sigma_1\tilde{\sigma}_1}\right)\right]dudv, \tag{62}$$

$$\mathcal{D}v = \frac{1}{\sigma_1\sqrt{2\pi}}\exp\left(-\frac{v^2}{2\sigma_1^2}\right)dv. \tag{63}$$

The free energy of the followed state can be obtained by plugging expressions (A18) and (A10) into Eqs. (35) and (36) and getting

$$-\beta_a f = \frac{1}{4}\beta_a^2 J^2(p-1)\left(\tilde{q}_1^p - 2x\frac{\beta_e}{\beta_a}c^p\right) + \frac{1}{4}\beta_a^2 J^2 - \frac{1}{4}\beta_a^2 J^2 p\tilde{q}_1^{p-1} + \frac{\int \mathcal{D}\{u,v\}\cosh^x(\beta_e v)\log[2\cosh(\beta_a u)]}{\int \mathcal{D}v\ \cosh^x(\beta_e v)}. \tag{64}$$

The energy is then obtained by deriving $e=\partial(\beta_a f)/\partial\beta_a$. Again, these equation are similar to standard replica equations with a kind of a ferromagnetic bias but do not have as simple form as was given by the mapping on Nishimori line for $T_e > T_K$.

D. What happens when one follows states: Turning cartoons into data

So far we were describing ideas and the formalism for the method of adiabatic following of Gibbs states. In the remaining of this section we describe and discuss results which can be obtained about the energy landscape and the structure of states for the fully connected p-spin model based on the previously derived equations.

One obvious application of the states following method is to compute how does the energy of equilibrium states evolve with temperature. Such energy-temperature diagrams (volume or entropy is sometimes plotted on the y axis or density is plotted as a function of the pressure) appear in many works about glassy systems,[20] for recent examples see Refs. 63 and 64. Except for a few very simplistic models such as the spherical p-spin models,[2,3,7] the random energy or random entropy model[6] or the random subcube model[9] (where the dynamics is exactly solvable), all these diagrams were drawn as qualitative schemes, or as results of Monte Carlo simulations. Moreover, in the field of glassy dynamics, the energy landscape is often cartooned by drawing many valleys of different sizes and depths. The states following method allows to draw the above mentioned figures with

actual quantitative data for any model solvable via the cavity or replica method.

The left part of Fig. 4 shows how does the energy of states depend on the temperature T_a. The (blue) continuous line that crosses the diagram is the equilibrium energy of the system at a given temperature. This curve is divided into four parts, the part above the dynamical temperature T_d represents a high-temperature liquid phase. Between the dynamical T_d and Kauzmann T_K temperature is the dynamical glass phase, where the free energy or energy are still given by the liquid result, but the equilibrium state is divided into exponentially many Gibbs states. Below the Kauzmann temperature T_K the static line is obtained by solving the 1RSB Eqs. (44)–(48), at this point its derivative changes discontinuously. This 1RSB solution becomes unstable below the Gardner temperature T_G (Refs. 23 and 60) below which the line is dashed, as it is no longer exact, the correct FRSB energy would be higher.

Each of the red lines (five roughly parallel lines crossing the figure) is obtained by following the evolution of one of the exponentially many states equilibrium at some $T_K < T_e < T_d$. When the state is heated the energy grows up to a spinodal point where the state disappears, i.e., when the only solution of Eqs. (40) and (41) with J_0 given by Eq. (52) has $m=0$. As T_e approaches T_d the spinodal point is at lower and lower temperatures, states very near to T_d are lost almost immediately when heated. This is an interesting result as in the spherical models, the state at T_d could be heated to much larger temperatures: that is an unphysical property of the spherical model that disappears in the Ising model we have considered here.

When the state is cooled down, the energy is decreasing, but slower than the equilibrium energy. As soon as the temperature changes the state goes out of equilibrium: this corresponds to the notion of glassy states trapping the dynamics up in the energy landscape. In Fig. 4 left we plotted the energy of states supposing they are stable against replica symmetry breaking. We found, however, that this was not always the case and thus denoted the unstable, thus unphysical, part of the curves by dashing. Indeed, the dashed part of the lowest state curve even crosses the equilibrium line, which is unphysical, a clear sign that the replica symmetry is broken. The left ends of the red lines (five roughly parallel lines) correspond to another spinodal point, in the sense that the nontrivial, $m \neq 0$, solution of the RS state following Eqs. (40) and (41) ceases to exist. This spinodal point does, however, not have a physical interpretation, as the states are unstable toward RSB in that region. We will see in Sec. V F that this unphysical spinodal is related to a known problem in the spin glass with ferromagnetic bias.

The right-hand side of Fig. 4 depicts the same quantities as the left-hand side, the difference is that for the adiabatic evolution of states we used the 1RSB Eqs. (44)–(48). The part where this changes the result is distinguished by dashing. We checked that even the 1RSB description of the states is not stable toward more steps of RSB so that the exact description of the dashed parts requires a full RSB solution. The 1RSB result, however, gives a much better—and physical—approximation of the correct behavior. Still, for the upper states a nonphysical spinodal point remains; this can be seen on the highest (red) curve when its dashed part finishes and turns into dotted (green), we will describe in Fig. 4 how the (green) dotted line was obtained. Obtaining the FRSB is only a technical problem of solving the corresponding equations as the mapping to the partly ferromagnetic model, Eq. (52), is valid on any level of RSB.

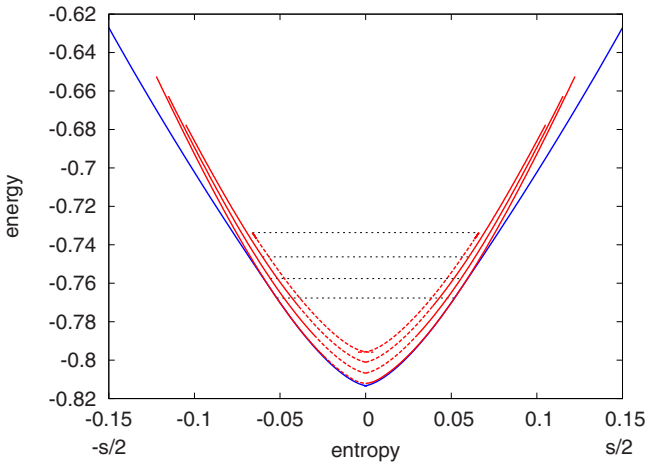

FIG. 5. (Color online) A direct quantitative look at the shape of states in the energy landscape of the fully connected three-spin model. The energy of four different states is plotted as a function of their entropy; we plot $s/2$ and $-s/2$ such that the width corresponds to the entropy. The shapes of the curves show how the valleys look in the energy landscape. The outermost curve (blue) is the total equilibrium energy versus entropy. The four inside red curves correspond to different states that are at equilibrium at temperatures $T_e=0.6815, 0.67, 0.66, 0.6513$, and their equilibrium energy e_e are marked by horizontal (black) dotted lines. The highest bottom of these states marks a lower bound on the best possible limiting energy for a slow annealing.

Note that our results correspond well to the solution of the dynamical equations in the spherical approximation, where indeed the transition toward more steps of replica symmetry breaking was observed:[3,7] we expect actually this behavior to be quite universal and to be observed in any spin-glass model with an 1RSB equilibrium solution.

One comment is in order here. The reader familiar with the phenomenology of the p-spin model will certainly find many similarities between our results and the one advocated in Ref. 65. In that work, the authors considered, like us, the states that are at higher free energies than the equilibrium ones for a given temperature T, and found that at high energies these states are always unstable toward RSB, just as we see in Sec. V G 2. Later on Crisanti *et al.*[66] clarified the nature of these high metastable states. There is, however, a major difference between our works: in Refs. 65 and 66 the authors were looking at the *typical* excited states at a given free energy f and temperature T, that is, at the most numerous ones. In our present work we instead concentrate on following the states that were typical at a given temperature. The point is that as soon as the temperature is changed, these states become out of equilibrium and not typical. If one wants to focus on the states that are the most important ones for the free-energy landscape, it is *necessary* to consider their basins of attraction, as we do, and this is why we have developed the following state method in the first place. We will

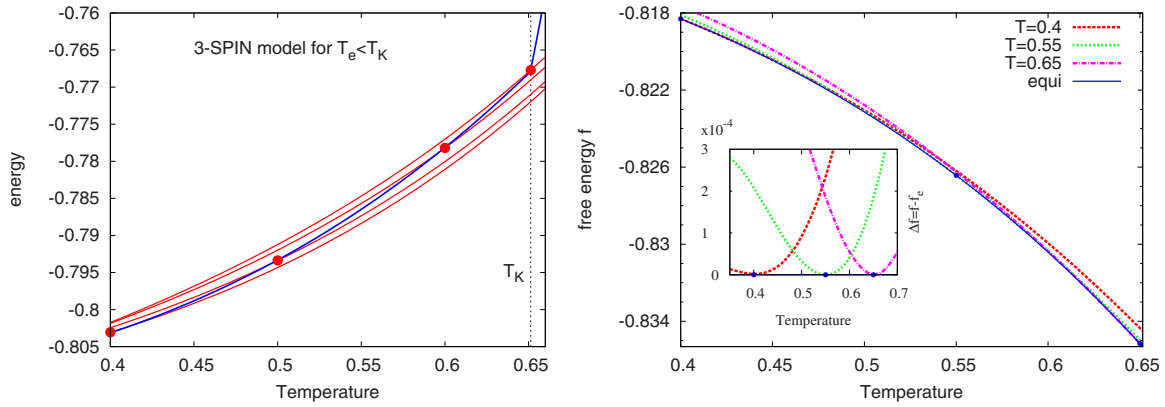

FIG. 6. (Color online) Explicit demonstration of the presence of temperature chaos below the Kauzmann temperature in the fully connected three-spin model. Left: the energy as a function of temperature for states below the Kauzmann transition: the four curves correspond to temperatures $T_e=0.4,0.5,0.6,0.6513$. Right: the crossing of free energies of different states as a function of temperature. The lower envelope (blue) is the equilibrium free energy: it results from the crossings of many states; here we show three such states that are the equilibrium ones at temperatures $T_e=0.4,0.55,0.65$. Inset: to make the crossing more evident, we plot the difference between the free energy of these three different states and the equilibrium free energy.

come back on this point when we will discuss the isocomplexity approach in Sec. VI C.

Figure 5 presents the same data as Fig. 4 in a different perspective. It is a sort of direct look at the shape of states in the energy landscape. The y axis is still the energy, the x axis depicts the size (entropy) of the state. More precisely we plot a line at $-s/2$ and $s/2$. The blue (outermost) line is the entropy of the equilibrium (static) solution. The four upper red lines correspond to different Gibbs states. The horizontal dashed lines depict energy at which these states are the equilibrium Gibbs states. Note that according to the laws of thermodynamics the derivative of the energy at the minima have to be zero, whereas Fig. 5 shows a slight nonphysical cusp. This is dues to the 1RSB approximation that underestimates the entropy, the FRSB solution would have the correct derivative.

E. Below the Kauzmann transition: Level crossings and temperature chaos

We now turn to the description of static spin-glass phase, $T<T_K$. Figure 6 uses equations derived in Sec. V C and depicts the evolution of states that are at equilibrium below T_K. Figure 6 left gives the energy as a function of temperature for three states that are at equilibrium (marked by red points) at some temperature $T_e<T_K$. In Fig. 6 right, we plot the free energy of these states as a function of temperature, the lower envelope of the free energies of all the states is then the equilibrium free energy. In order to enhance the differences, in the inset, we subtracted the equilibrium free energy from the free energies of the three states.

These plots clearly show that, although a finite number of states dominates the partition sum (which is the very

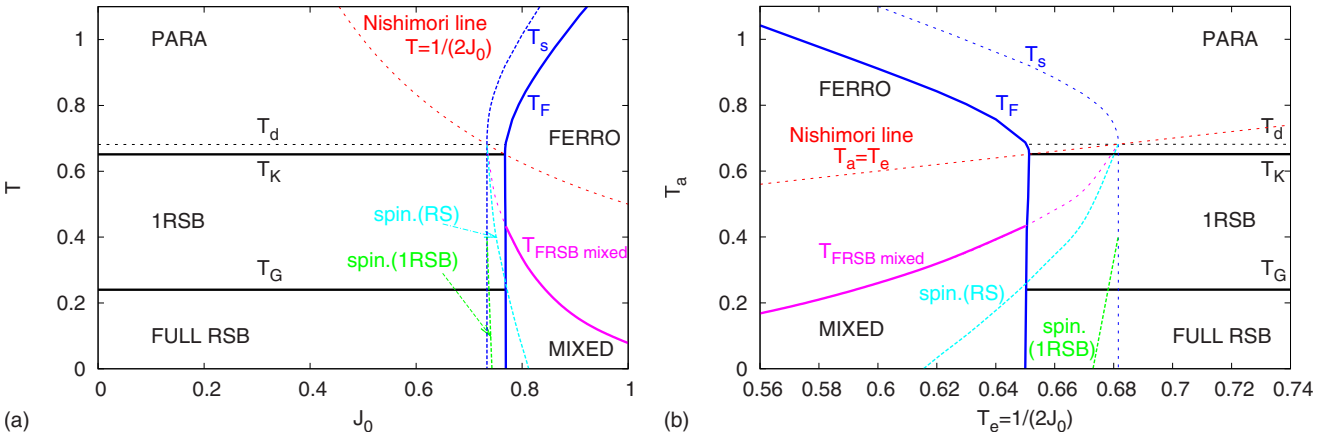

FIG. 7. (Color online) The phase diagram of the fully connected three-spin model with a ferromagnetic bias (left), or equivalently, the phase diagram in function of the two temperatures T_a and T_e in the state following formalism. True phase transitions are marked by thick lines while spinodals and the Nishimori lines are drawn thin and dashed. The two phase diagrams are given to highlight how the physics of states following can be understood intuitively from the ferromagnetically biased model. Note that the line denoting the transition from spin glass to ferromagnet (computed at the 1RSB level) is almost but not completely straight.

definition of the glass phase below T_K), these states become out of equilibrium as soon as the temperature is slightly changed. Even though for all $T<T_K$ the partition sum is dominated by a finite number of state: *these states change entirely when the temperature is slightly modified*. This is the phenomenon of temperature chaos that appears due to free energy levels crossing.

Temperature chaos has been discussed extensively in spin glasses, see, for instance,[67–71] it is crucial in the interpretation of memory and rejuvenation experiments.[72,73] Its existence was a subject of debates, as its absence was advocated in many papers,[74–76] as well as its presence.[77–80] Our results allow to finally clearly demonstrate that temperature chaos is present in the Ising fully connected p-spin models, and that it arises through many level crossings, as advocated in Refs. 6 and 8.

F. Phase diagram of evolving states and the mapping to a ferromagnetic p-spin model

As we derived in Secs. III F and V B, all the physics of the adiabatic evolution of equilibrium states above the Kauzmann temperature for the $J_0=0$ p-spin model can be induced from the known, see, e.g., Refs. 56 and 57, phase diagram of the $J_0\neq 0$ p-spin model. We will now discuss the phase diagram in the context of results given in Figs. 4 and 5. Figure 7 shows two drawings of the same phase diagram, the y axis in both is the actual temperature. The x axis on the left is the standard ferromagnetic bias J_0, on the right the x axis is the associated equilibrium temperature $T_e=J^2/(2J_0)$ (in both figures we took $J=1$). The red (dashed) line in both parts is $T_a=T_e=J^2/(2J_0)$, on the left this is the Nishimori line, on the right this is the equilibrium line. The task is to follow states that are the equilibrium ones on this line for $T_e\geq T_K$. The horizontal black lines depict the location of the dynamical, Kauzmann and Gardner temperatures for T_a.

The phase diagram of the p-spin model with a ferromagnetic bias J_0, Fig. 7 left-hand side see also Refs. 56 and 57, has five thermodynamic phases separated by thick lines in the figure: the paramagnetic phase at high temperature (PARA). The 1RSB spin-glass phase for low enough bias J_0 and $T<T_K$ that becomes a full RSB phase for $T<T_G$. The ferromagnetic phase (FERRO) for J_0 large enough and $T<T_F$ that becomes a mixed phase with both ferromagnetic and full RSB order (MIXED) for $T<T_{\mathrm{FRSB\ mixed}}$. At low enough J_0 the system is a spin glass with an ergodicity breaking transition at T_d and then the Kauzmann and Gardner phase transitions at T_K and T_G. At larger J_0, the system undergoes a first-order ferromagnetic transition at T_F. The ferromagnetic state is thermodynamically stable starting from the spinodal temperature $T_s>T_F$, at T_F it becomes thermodynamically dominant. Below the pink line, $T_{\mathrm{FRSB\ mixed}}$, the replica symmetric solution describing the ferromagnetic state ceases to be stable toward RSB and the system transits into the FRSB mixed phase. The mixed phase has some unphysical spinodals: below the light blue, spin.(RS), line there is no nontrivial ferromagnetic RS solution. This is cured by the 1RSB approach, but only down to the green, spin.(1RSB), line below which there is no nontrivial ferromagnetic 1RSB solution. The correct spinodal should be a vertical line in the FRSB computation. The Nishimori line is the red dashed curve: notice how it crosses the ferromagnetic transition exactly when $T_F=T_K$ and the spinodal at $T_s=T_d$.

The right-hand side of Fig. 7 depicts the same diagram as a function of the equilibrium temperature T_e. Following a state at equilibrium at temperature T_e to temperature T_a is equivalent to looking to the ferromagnetic state on the Nishimori line at T_e, and then moving vertically to other temperatures T_a. The vertical strip of temperatures $T_K\leq T_e\leq T_d$ is hence particularly relevant for state following. The (blue) spinodal ferromagnetic line T_s thus corresponds to the high-temperature spinodal line in state following (see Fig. 4). The (pink) line $T_{\mathrm{FRSB\ mixed}}$ corresponds to the point where the state divides into many substates and develop a (presumably) full replica symmetry breaking. However, we are unable to follow the state with the RS formalism below the light blue line that corresponds to an unphysical spinodal. This is cured in part by the 1RSB formalism, but the same problem arises in this case below the green line, so that a FRSB solution is eventually needed to describe the adiabatic evolution of states at $T_e=T_d$.

For $T_e<T_K$ $[J_0>J^2/(2T_K)]$ the phase diagram shows a ferromagnetic phase which would correspond to following a state that almost surely does not exist for a typical instance of the problem. To follow states equilibrium below T_K the mapping to a model with a ferromagnetic bias breaks.

Two comments are in order about the spinodal and the ferromagnetic transition. Let us first discuss the spinodal, which we believe to be vertical below T_d: the FRSB ferromagnetic solution in the mixed phase must exist up to the vertical (blue) line. However, different levels of replica symmetry breaking have different unphysical spinodal lines beyond which no nontrivial ferromagnetic solution exist at the corresponding RSB level (the blue spinodal for RS and green for 1RSB are depicted). Such behavior is not unheard of: the very same phenomena takes place in the study of the Sherrington-Kirkpatrick model in external magnetic field[81] (that is, for $p=2$). There also the boundary of the mixed phase is a vertical line in the FRSB solution but differs at all finite levels of RSB.[15,82] Similar features were observed in the dilute mean-field spin glasses as well.[83,84] In the state following method the lack of a ferromagnetic solution near to the true FRSB spinodal translates into difficulty of obtaining a sensible 1RSB upper bound on the low-temperature adiabatic evolution of states with $T_e\approx T_d$.

Let us now consider the ferromagnetic transition line T_F below the Nishimori line. Nishimori proved[56] that the line was either vertical or bending toward the ferromagnetic phase, this is also apparent from the states following interpretation. Although it might not be completely visible from Fig. 7 (left), the analysis of the 1RSB equations shows that the line is bending slightly toward larger J_0 as T is lowered, although the effect is very small (to the best of our knowledge, this was an unknown feature of this phase diagram). Interestingly, this has a clear interpretation in the states following formalism. At zero temperature, the energy of the ferromagnetic state at $J_0=1/(2T_K)$ is equal to the bottom energy of the equilibrium state at T_K. As discussed in Sec. V E chaos and level crossings make these states to have a

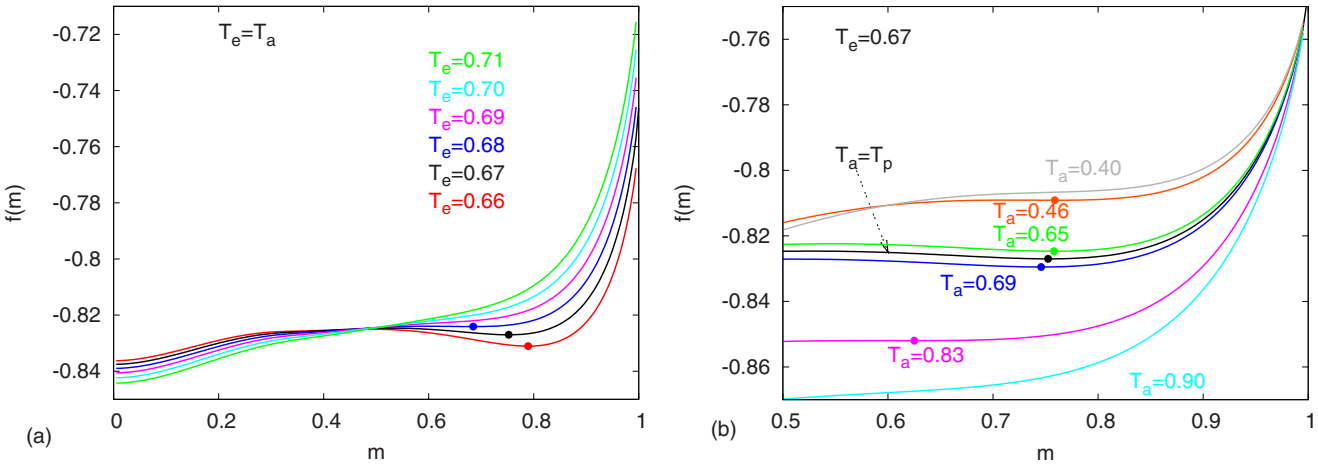

FIG. 8. (Color online) The replica symmetric free energy of a state at temperature T_a as a function of the distance m from an equilibrium configuration at T_e in the three-spin fully connected model. The points indicate the minima corresponding to what the state following method finds. Left: in this case $T_a=T_e$; a minimum starts to form around the equilibrium configuration for $T_e<T_d=0.6815$ while in the liquid phase $T_e>T_d$ no such minimum exists. Right: we now use $T_a\neq T_e$ (here $T_e=0.67$) and we observe how the curves are evolving with T_a. Upon warming, the minimum happens at lower free energies and m is decaying, indicating that the state gets larger until finally a spinodal point is reached and no more minimum exist; this is the moment where the state melts into the liquid. Upon cooling, we thus expect that both the free energy and m increase. This is indeed the case but for low temperature (here $T_a=0.46$) we start to observe a nonmonotonous behavior for m. Worse, if the temperature is again lowered (here $T_a=0.4$) the minimum disappears. These are nonphysical features and are clear signs that replica symmetry must be broken for low temperatures.

larger energy than the true equilibrium one at $T<T_K$; as a consequence, the ferromagnetic state at $T=0$ and $J_0=1/(2T_K)$ *must* have bottom energy larger than the ground-state energy of the system, so that the ferromagnetic transition can only happen for larger values of J_0. Interestingly chaos disappears in the large p limit (as well as in the spherical approximation) and this is why this line is strictly straight in the phase diagram of the random energy model[36] and in the spherical p-spin model.[85] Note that there had been a considerable amount of efforts to discover this effect in finite-dimensional spin glasses, see, for instance, Ref. 86 and it is therefore interesting to observe it in mean-field models as well.

G. Relation to the Franz-Parisi potential

The idea of exploring one of the many phases in glassy mean-field systems is a very natural one and is therefore not new. Our states following approach is actually related to the one pioneered by Franz and Parisi years ago,[3,28,87,88] which is now commonly referred to as the *Franz-Parisi potential*. Their idea was to study glassy systems in presence of an attractive coupling among two real replicas, one of which being at equilibrium. Looking to the free energy of the copy when its overlap with an equilibrium configuration is tuned allows to compute the local free-energy potential around this equilibrium point.

What the states following method is actually doing is to focus directly on the minimum of the Parisi-Franz potential, thus bypassing the need of an attractive coupling and making the formalism much simpler and applicable easily to the models on sparse graphs. The Franz-Parisi potential can, however, be obtained within the states following method if we fix the overlap between the state at temperature T_e and T_a. The purpose of the present paragraph is to explain how to do this in the p-spin model. The reason is twofold: (a) we want to make the correspondence with the Franz-Parisi formalism and (b) looking at these free energies turns out to be extremely instructive to understand the unphysical spinodal points and related issues discussed in the previous section.

Conveniently enough, in our mapping to a model with an effective ferromagnetic coupling J_0, the magnetization parameter m, Eq. (40), is nothing else than the overlap of the configuration under study and the planted one. This demonstrates the usefulness of the above mapping. The free energy at fixed magnetization of a p-spin model with a ferromagnetic bias J_0 at the temperature T is equal to the Franz-Parisi potential for the spin-glass problem with temperature $T_e=J^2/(2J_0)$ and $T_a=T$.

Fixing the magnetization, i.e., ensuring $\Sigma_i s_i/N=m$, is done by introducing a Lagrange multiplier h and writing the partition function of the system with a fixed magnetization as $Z_m=Z_h e^{-N\beta hm}$, where Z_h is a partition function of the model with an external magnetic field, i.e., with Hamiltonian $H_h=H-h\Sigma_i s_i$. Once we compute the free energy of the model with an external magnetic field $f(h)$ the free energy of the system with magnetization fixed to m is recovered via $f(m)=f(h)+hm$. To fix a value $m=m^*$ we need to ensure that $\partial f(h)/\partial h|_{h^*}=-m^*$; the $f(m)$ is thus a Legendre transform of $f(h)$.

This allows us to derive easily the Franz-Parisi potential in the p-spin model. Actually, it also allows to obtain instantaneously all the (not straightforward) Franz-Parisi computations in the spherical and mixed spherical p-spin models just by looking to the equilibrium free energy of the model with a ferromagnetic bias. The reader is invited, for instance, to compare the free energy in Ref. 85 with the Franz-Parisi potential in Refs. 3 and 88.

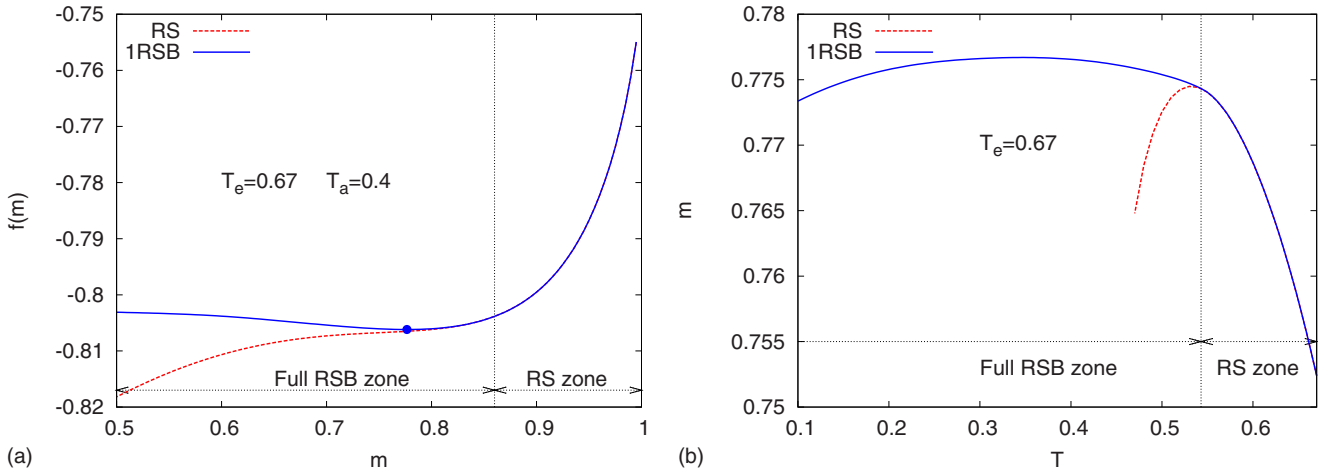

FIG. 9. (Color online) Left: comparison between the RS Franz-Parisi potential lower curve (red) and the 1RSB one upper curve (blue). The point marks the minima on the 1RSB curve. Right: magnetization of the minima as a function of temperature T_a. Again the lower (red) curve is the RS result, the upper (blue) curve is the 1RSB result. The increasing or nonexisting part of the curve in unphysical, the size of the unphysical region is much smaller in the 1RSB result.

1. Franz-Parisi potential at the replica symmetric level

At the RS level, the equations for the p-spin model with an external field h become

$$m = \int_{-\infty}^{\infty} \mathcal{D}y \tanh(\beta_a J y \sqrt{pq^{p-1}/2} + \beta_a J_0 p m^{p-1} + \beta_a h), \tag{65}$$

$$q = \int_{-\infty}^{\infty} \mathcal{D}y \tanh^2(\beta_a J y \sqrt{pq^{p-1}/2} + \beta_a J_0 p m^{p-1} + \beta_a h) \tag{66}$$

with $\mathcal{D}y = dy e^{-y^2/2}/\sqrt{2\pi}$. The free energy is given by Eq. (42) with $\beta_a h$ added in the argument of the cosh.

Note that when the free energy is nonconvex (as it is in the present case), one has to be extremely careful in solving these equations. Indeed if one simply chooses h once and for all and simply performs a recursion of Eqs. (65) and (66) some values of m will never be obtained. A good method is to first choose the desired value m^* and then to fix the magnetic field h *at each iteration* such that Eq. (65) is satisfied. This can be easily generalized in the 1RSB equation. In Fig. 8, we show the results of this procedure.

The left side of Fig. 8 shows the free energy of configurations at a distance m from the planted one in the ferromagnetically biased model; this is the Franz-Parisi potential. One sees that for $T_e > T_d = 0.6815$ there is no minimum except the trivial one at $m=0$; for $T_e < T_d = 0.6815$, however, a second minimum appears with a finite value of the overlap: this is precisely the one found in the states following approach, which is only performing a gradient descent in this free energy starting from the point $m=1$, thus directly focusing on the nontrivial minima of the free-energy potential.

The right-hand side of Fig. 8 shows the free energy of configurations at a distance m from the planted one when the temperature is different from the planted temperature. We have used $T_e = 0.67$ and we can see how the free energy of the state changes with temperature. This is actually very instructive. When rising the temperature the free energy of the state decreases (as a free energy should with temperature because of the positivity of entropy) while the overlap m at the minimum gets smaller: this is the sign that the state becomes larger. At even larger temperature, a spinodal point is met and the minimum (as well as the state) stop to exist.

When decreasing the temperature, we expect that both the free energy and m increase, as the state gets smaller and deeper in the free-energy landscape. This is indeed the case initially but for low temperatures (here $T_a = 0.46$) we start to observe a nonmonotonous behavior for m. If the temperature is further lowered (here $T_a = 0.4$) the minimum disappears, as we have seen in the previous section. These are nonphysical features that show that the replica symmetric assumption is incorrect and that we need to break the replica symmetry.

2. Franz-Parisi potential at the replica symmetry broken level

To obtain the 1RSB approximation of the Franz-Parisi potential we need to fix the parameter m in the 1RSB equations using again an auxiliary magnetic field h. The result for $T_a = 0.4$ and $T_e = 0.67$ is shown in Fig. 9 left. The lower line (red) is the replica symmetric result, the upper line (blue) is the 1RSB result. The two curves differ in the RS unstable zone on the left side of the plot. Unlike the unstable RS result, the 1RSB Franz-Parisi potential has a secondary physical minimum at about $m = 0.776$. Moreover, as general in replica theory, the 1RSB free energy is always larger than the RS one.

Right part of Fig. 9 shows the dependence of the magnetization at the minimum as a function of temperature T_a. The state following method becomes studying the ferromagnetically biased model, in ferromagnets magnetization usually grows as the temperature decreases. Hence, the part where $m(T_a)$ increases (or does not exist) is unphysical and will disappear in the FRSB solution. We can see that the physical

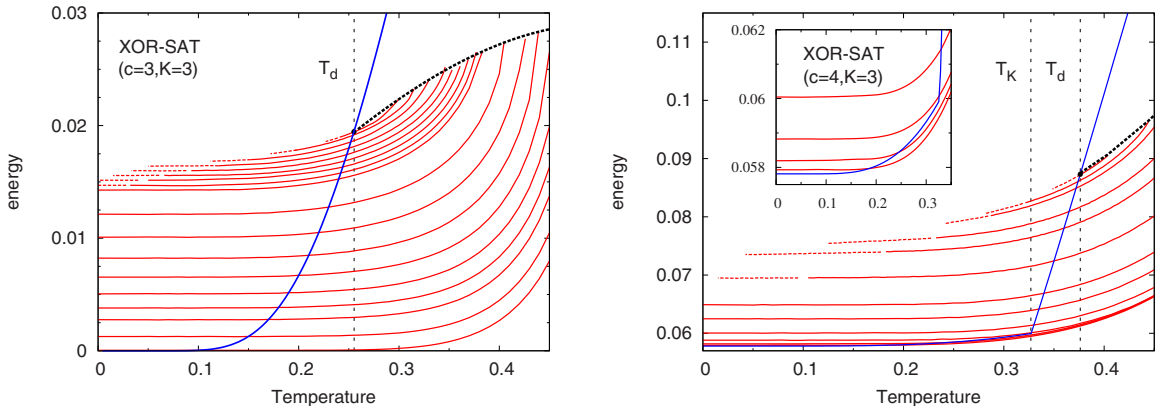

FIG. 10. (Color online) Representative behavior of states in diluted mean-field systems. Left: the XOR-SAT problem with $K=3$ and $c=3$. Right: the XOR-SAT problem with $K=3$ and $c=4$. The value of energy here is the number of violated constraints per variable. The blue line crossing the diagram is the equilibrium energy computed from the standard cavity method, Eqs. (16)–(21). The vertical lines denote the dynamical and Kauzmann temperatures. The red lines depict adiabatic evolution of states that are the equilibrium one at the temperature T_e where the red curve crosses the blue one. The state evolution curves are obtained by solving Eqs. (24)–(26) when $T_e \geq T_K$ and Eqs. (32)–(37) when $T_e < T_K$ (in the inset of the right-hand side). The dashed part of the red curves depicts the region of temperatures where the state is no longer stable toward replica symmetry breaking and splits into many substates. The ends of the red curves at nonzero temperature correspond to the nonphysical spinodal points beyond which Eqs. (24)–(26) have only the trivial liquid solution.

region extends into lower temperatures T_a for the 1RSB result. We also observed that the 1RSB magnetization is systematically larger than the RS one.

The above findings suggest a method how to obtain a lower bound on the energy of the state even at temperatures where the 1RSB solution does not exist (the 1RSB Franz-Parisi potential does not develop the secondary minima). At such temperature T_a the magnetization at the real minima (which we would observe in the FRSB result) have to be larger than the maxima of magnetization m_m in the 1RSB result over all T_a. As the FRSB free energy is larger that the 1RSB one the free energy at that minima have to be larger than the 1RSB free energy at m_m. Using this receipt we can thus obtain a lower bound on the free energy (and energy) which is probably not far from the true result. This is how we obtained the green dotted part in Fig. 4.

Note, however, that the above described construction of the lower bound is not very elegant and requires the calculation of the full Franz-Parisi potential $f(m)$. It is interesting to see if a better approximation to the FRSB result can be obtained using different techniques.

VI. SECOND APPLICATION: ENERGY LANDSCAPE IN CONSTRAINT SATISFACTION PROBLEMS AND DILUTED MODELS

We have discussed at length the various aspects of adiabatic evolution of Gibbs states for the simple case of fully connected p-spin model because many of those aspects repeat for the computationally more involved models on sparse random graphs such as XOR-SAT or graph coloring. In this section we present results for those two models.

A. Following states in diluted spin models

In Fig. 10 we plot the energy of states versus temperature for the three-XOR-SAT problem with degree of variables $c=3$ (left) and $c=4$ (right). The behavior is extremely similar to the one of the fully connected model and the very same features are observed: the spinodal upon heating, the transition toward symmetry breaking upon cooling, and the unphysical spinodal. Note that these plots have been obtained with the RS procedure and a first remark is that the RS computation gives a more complete result than in the fully connected case. Since equilibrium states *do not* develop the Gardner instability, it is not surprising that the instability

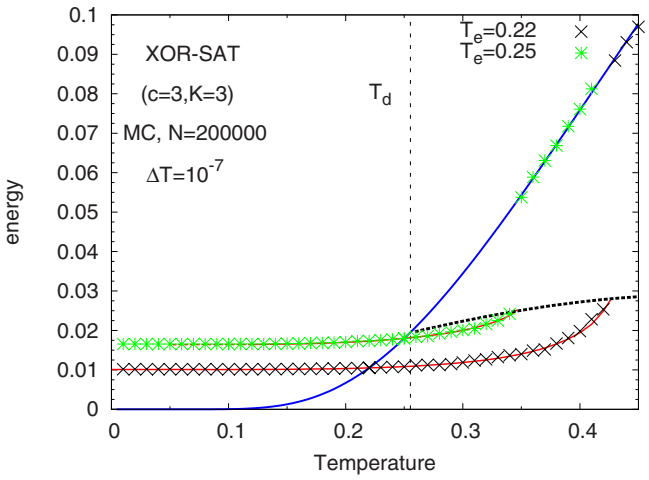

FIG. 11. (Color online) Following states in the XOR-SAT problem with $c=3$ and $K=3$ with Monte Carlo simulations. On this picture, we have reproduced the data of Fig. 10 with Monte Carlo simulation (black and green crosses). We have prepared a large XOR-SAT system at equilibrium for $T=0.25$ and $T=0.22$ and performed slow cooling and heating with a Monte Carlo procedure: when the dynamics is slow enough (we have changed the temperature only by a factor $\Delta T=10^{-8}$ at each Monte Carlo step) the energy in the simulation follows perfectly the predictions of the states following formalism. We have thus succeeded in predicting the adiabatic evolution of the dynamics starting from equilibrium.

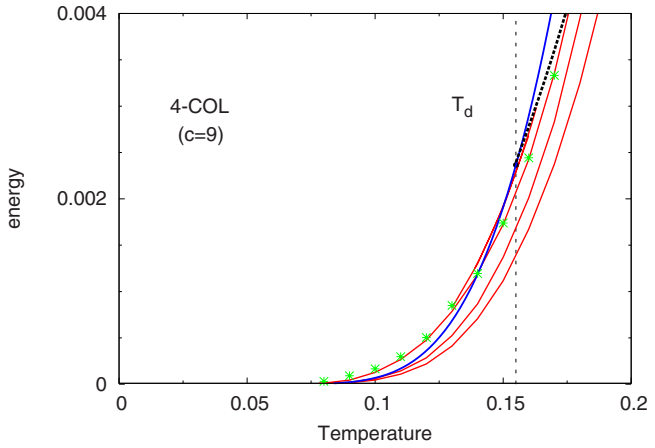

FIG. 12. (Color online) State following for the four-coloring of nine-regular random graphs. Equilibrium in blue, several states in red. Unlike in the XOR-SAT problem, here the states descent very fast to zero energies. Asterisk (green) represent the results of adiabatic simulations starting from an equilibrated configuration on a $N=10^5$ graph and then using the BP equations initialized in the equilibrated configuration for different temperatures: the energy follows again the prediction of the states following formalism.

toward RSB is less strong in the out-of-equilibrium states as well. However, we observed once again that the states at equilibrium close to T_d undergo a FRSB transition and decompose into many marginally stable substates: this seems to be a universal features of spin glasses.

In order to check these results, we have performed the following numerical simulation. We have first prepared two large XOR-SAT system with $c=3$ and $K=3$ and $N=200\,000$ spins at equilibrium for temperature $T=0.22$ and $T=0.25$. Of course, since these temperatures are below the dynamic transition, this would be an impossible task if we could not use the planting trick described in Sec. III E that allows to prepare at virtually no computational cost a random instance *together* with an equilibrated configuration. Then, we have used a metropolis Monte Carlo algorithm initialized in the planted configuration to follow the state upon slow cooling and slow heating. As shown in Fig. 11, the results of the simulation agree perfectly with the theoretical predictions, including the location of the high-temperature spinodals. We have also tried to use the BP equations on a single given graph initialized in the planted configuration instead of using Monte Carlo simulation. As seen in Fig. 12, this also yields a perfect agreement.

As already pointed out computing the limiting energy of adiabatic simulated annealing corresponds to the zero temperature $T_a=0$ energy of a typical state with $T_e=T_d$, and this requires to consider replica symmetry breaking within the states. At least the 1RSB computation plus the analysis suggested in Sec. V G 2 is needed to compute lower bounds on the energy achieved by the infinitely slow annealing. This is numerically involved and we will thus address it in subsequent works. Another way of accessing this energy value would be to solve the dynamical equations,[20,89–91] which at current time seems to be even much harder task. Despite these limitations, a very useful insight about the energy landscape and limitations of simulated annealing and other stochastic local search algorithms can be obtained from the results that we already have from the states following method, as we explain in the next section.

B. Canyon versus valleys

Let us turn our attention to Fig. 12. It depicts in the same manner as before the evolution of states for the four-coloring of nine-regular random graphs. Unlike in the examples in Fig. 10 we see that all depicted states fall very fast down to

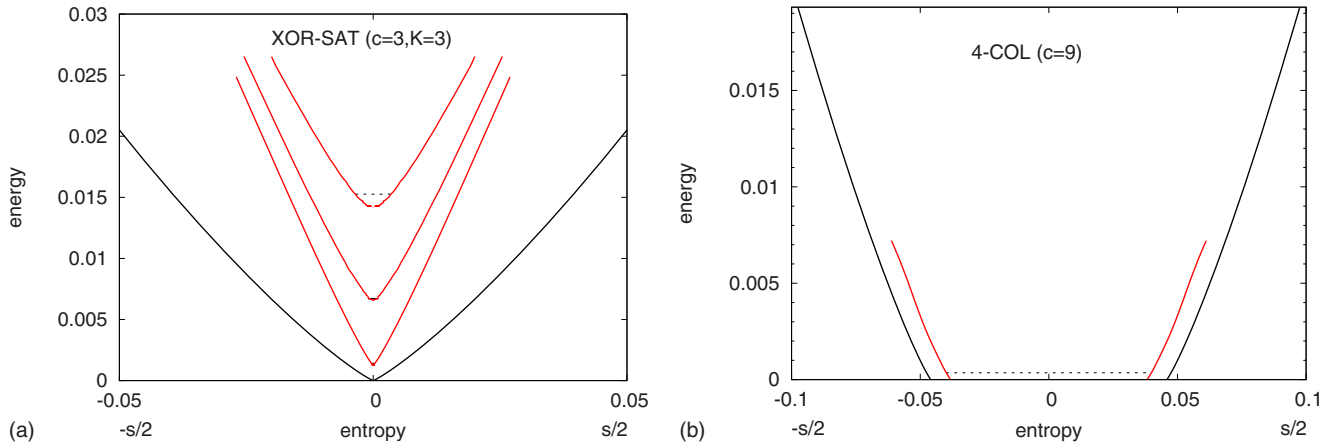

FIG. 13. (Color online) Data from Figs. 10 and 12 plotted in order to visualize the energy landscape. The energy e is plotted against the entropy $s=\beta_a(e-f)$ for different equilibrium states. We plotted $s(e)/2$ and $-s(e)/2$ such that the width corresponds to the logarithm of the number of configurations at energy e for the Gibbs state. Left: XOR-SAT with $c=3$ and $K=3$. Right: four coloring of random graphs with $c=9$. The black curve corresponds to the equilibrium total entropy. The red curves are different equilibrium states, corresponding to $T_e=0.15, 0.2, 0.24$ (left) and $T_e=0.12$ (right), the energies corresponding to T_e are depicted by horizontal black dashed lines. The left-side states, with their finite-energy bottoms, remind us of the valleys in Fig. 1 while the right side reminds of deep canyons that all reach the ground-state energy level. Note that our distinction between canyons and valleys is purely energetic, both canyons and valleys can have both zero or positive bottom entropy.

zero energy. Again due to RSB instabilities, so far, we are not able to show explicitly that the state with $T_e=T_d$ goes down to zero energy. But in any case we see that the asymptotic behavior at zero temperature is rather different.

In order to be precise, we now distinguish between two types of states:

(a) canyons are states with bottoms at the ground-state energy.

(b) Valleys are states with bottoms strictly above the ground-state energy.

By definition, there is at least one canyon state in every system. The definition is rather intuitive when looking to the cartoon of the energy landscape in Fig. 1. The difference between canyons and valleys is accentuated in Fig. 13 where data from Figs. 10 and 12 are plotted in order to visualize the shape of the states. The energy is plotted against the entropy $s=\beta_a(e-f)$ for different equilibrium states. We plotted $s(e)/2$ and $-s(e)/2$ such that the width corresponds to the logarithm of the number of configurations at energy e for the Gibbs state. The left-hand size is for the $c=3$ three-XOR-SAT, right-hand side for four-coloring of nine-regular random graphs. The black (the outermost) curve corresponds to the equilibrium energy and entropy. The different red curves are shapes of states equilibrium at energy e_e depicted by the horizontal dashed lines. The bottoms of depicted states on the left are at positive energy hence these states are valleys, whereas the bottom of the state depicted on the right is at zero energy, this is hence a canyon.

Based on the distinction between canyon states and valley states, we now describe two distinct types of energy landscape, depending on the basin of attraction of states at the dynamical transition $T_e=T_d$:

(a) in the canyons-dominated landscape, a typical equilibrium state at $T_e=T_d$ is a canyon.

(b) In the valleys-dominated landscape those states are valleys.

In the previous examples, the cases of the XOR-SAT problem we showed have valleys dominated landscape and the coloring example is canyons dominated. This has a deep algorithmic consequence: an adiabatically slow simulated annealing *is able* to find the ground state in the canyons-dominated landscape but *this is not the case* for the valleys-dominated landscape. In constraint satisfaction problems where one can change continuously the connectivity, we thus expect that there will be a *sharp transition* c_{cv} from the canyons-dominated landscape to the valleys-dominated landscape as the density of constraints is increased. This phase transition must happen between the clustering and satisfiability threshold, $c_d \leq c_{cv} \leq c_s$. We will now argue that the canyons/valleys transition c_{cv} is upper bounded by the rigidity transition introduced in Refs. 41 and 49.

C. Warning propagation limit and the bottoms of states

It is possible to derive analytical equations for the energy of the bottoms of equilibrium states, i.e., in the zero-temperature limit, $\beta_a \to \infty$. This is simply the limit of Eq. (24) that takes a simpler closed form when $T_a=0$. Here we present these equations and their derivation for the XOR-SAT problem. We also derived corresponding equations for the graph coloring.

We consider for simplicity that degree of every variable in the XOR-SAT problem is fixed to c and all interactions are antiferromagnetic $J_a=-1$. For our purpose it is convenient to rewrite Eq. (24) in terms of probability ε that a constraint is violated in the planted configuration, Eq. (15),

$$P_s(\psi) = \frac{1}{2^{K-2}} \sum_{\{s_i\}} [(1-\epsilon)\delta_{1,s+\sum_i s_i} + \epsilon \delta_{0,s+\sum_i s_i}] \int \prod_{i=1}^{K-1} \prod_{j=1}^{c-1} dP_{s_i}(\psi^j)\, \delta\{\psi - \mathcal{F}[(\psi^j)]\}, \tag{67}$$

where the sums in the Kronecker deltas are modulo 2 and $\mathcal{F}(\{\psi^j\})$ is defined by the BP Eq. (6) at zero temperature $\beta_a \to \infty$. In this limit we can write the warning propagation version of Eq. (67) which can be solved without the use of population dynamics.

Let us introduce the following probabilities: (a) μ is a probability that a given constraint is forcing variable into a value in which it was planted (warning from a to i). (b) η is a probability that a given constraint is forcing variable into a value in which it was not planted (warning from a to i). (c) $\tilde{\mu}$ is a probability that a variable is being forced into a value into which it was planted (warning from i to a). (d) $\tilde{\eta}$ is a probability that a variable is being forced into a value into which it was not planted (warning from i to a).

The following equations are then linking the above probabilities:

$$\tilde{\mu} = \sum_{s=0}^{c-2/2} \sum_{r=1}^{c-1-2s} \frac{(c-1)!}{s!(r+s)!(c-1-r-2s)!} \mu^{s+r} \eta^s (1-\mu-\eta)^{(c-1-r-2s)}, \tag{68}$$

$$\tilde{\eta} = \sum_{s=0}^{c-2/2} \sum_{r=1}^{c-1-2s} \frac{(c-1)!}{s!(r+s)!(c-1-r-2s)!} \mu^{s} \eta^{s+r} (1-\mu-\eta)^{(c-1-r-2s)}, \tag{69}$$

and

$$\mu = (1-\epsilon) \sum_{r=0}^{K-1/2} \frac{(K-1)!}{(2r)!(K-1-2r)!} \tilde{\mu}^{K-1-2r} \tilde{\eta}^{2r} + \epsilon \sum_{r=0}^{K-2/2} \frac{(K-1)!}{(2r+1)!(K-2-2r)!} \tilde{\mu}^{K-2-2r} \tilde{\eta}^{2r+1}, \tag{70}$$

$$\eta = (1-\epsilon) \sum_{r=0}^{K-2/2} \frac{(K-1)!}{(2r+1)!(K-2-2r)!} \tilde{\mu}^{K-2-2r} \tilde{\eta}^{2r+1} + \epsilon \sum_{r=0}^{K-1/2} \frac{(K-1)!}{(2r)!(K-1-2r)!} \tilde{\mu}^{K-1-2r} \tilde{\eta}^{2r}. \tag{71}$$

Sanity check is that the above equations give $\mu=[1-(1-\mu)^{c-1}]^{K-1}$ and $\eta=0$ when $\epsilon=0$, this is the equation for appearance of the hard fields derived in Ref. 49.

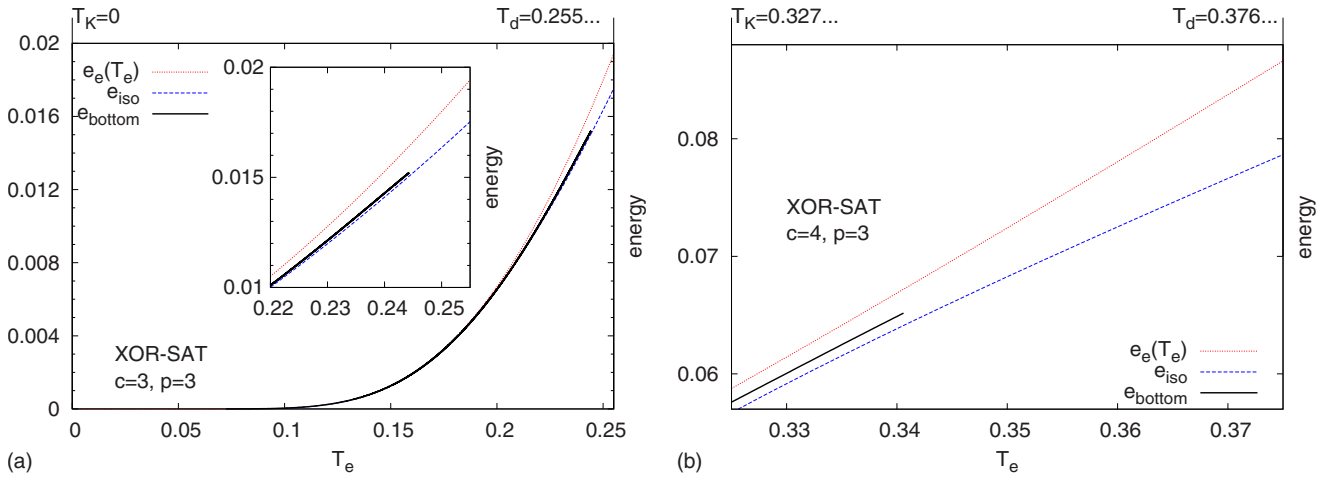

FIG. 14. (Color online) Comparison between the exact adiabatic evolution of states and the isocomplexity lower bound. The black line is the energy of the bottoms of states that were the equilibrium ones at temperature $T_K \leq T_e \leq T_d$ in XOR-SAT for $c=3$ and $K=3$ (left, the inset is a zoom) and for $c=4$ and $K=3$ (right). The red (uppermost) line is the equilibrium energy at T_e. The blue line is the isocomplexity lower bound from Ref. 5.

The corresponding energy is expressed as

$$E = \sum_{r=1}^{c/2} r P_{i+\partial i}(r) - c(1-1/K)P_a, \tag{72}$$

where $P_{i+\partial i}(r)$ is the probability that r contradictions happened when a variable i and all its neighbors are added. And P_a is the probability that a contradiction happened when the constraint a was added. We have

$$P_a = (1-\epsilon)\sum_{r=0}^{K-1/2} \frac{K!}{(2r+1)!(K-1-2r)!}\tilde{\mu}^{K-1-2r}\tilde{\eta}^{2r+1} + \epsilon\sum_{r=0}^{K/2} \frac{K!}{(2r)!(K-2r)!}\tilde{\mu}^{K-2r}\tilde{\eta}^{2r}, \tag{73}$$

TABLE I. Largest values of ϵ with a nontrivial solution of Eqs. (68) and (71) in the XOR-SAT problem on regular hypergraph with K-body interactions. This gives lower bounds to the largest possible values of the noise in the noisy reconstruction on trees.

K	c	ϵ	η	μ
3	3	0.01665(1)	0.088265	0.571804
3	4	0.05184(1)	0.094346	0.886841
3	5	0.09558(1)	0.128800	0.723037
4	3	0.00656(1)	0.011682	0.907334
4	4	0.03179(1)	0.059680	0.933018
4	5	0.06673(1)	0.087771	0.794195
4	6	0.08815(1)	0.123228	0.857183
5	3	0.00349(1)	0.006069	0.936580
5	4	0.02298(1)	0.043819	0.952231
5	5	0.05259(1)	0.068310	0.830129

$$P_{i+\partial i}(r) = \sum_{s=1}^{c-2r} \frac{c!}{r!(r+s)!(c-s-2r)!}\mu^{r+s}\eta^r(1-\mu-\eta)^{(c-s-2r)} + \sum_{s=1}^{c-2r} \frac{c!}{r!(r+s)!(c-s-2r)!}\mu^{r}\eta^{r+s}(1-\mu - \eta)^{(c-s-2r)} + \frac{c!}{r!r!(c-2r)!}\mu^r\eta^r(1-\mu-\eta)^{(c-2r)}. \tag{74}$$

The solution of these equations is depicted in Fig. 14 by a black line. Because of the relaxation within the state, the bottom is significantly lower than the equilibrium energy (red line).

Let us compare the state following result with an interesting heuristic idea to estimate the bottoms of states that was developed in Ref. 5 (see also Ref. 3). It uses an approach called isocomplexity. Instead of exactly following the states, the authors proposed instead to count the number of states at a given temperature T_e, and then to consider the energies at $T<T_e$ for which the number of state is equal to the one at T_e. Isocomplexity leads, however, only to a lower bound, because ending up at lower energies would be exponentially improbable. We see in Fig. 14 that indeed the true bottom is always at larger energy than given by the isocomplexity computation of Ref. 5.

Note also that above certain temperature T_e the equations do not have any nontrivial solution, this corresponds again to the nonphysical spinodal point that is observed in Fig. 10. The physical reason for this is that the states are unstable against RSB and that we should have used the RSB formalism. The noise level ϵ corresponding to this spinodal point is summarized in Table I.

D. Where the really hard problems really are?

We shall now argue that the canyons/valleys transition c_{cv} is upper bounded by the rigidity transition.[41,49] In the limit

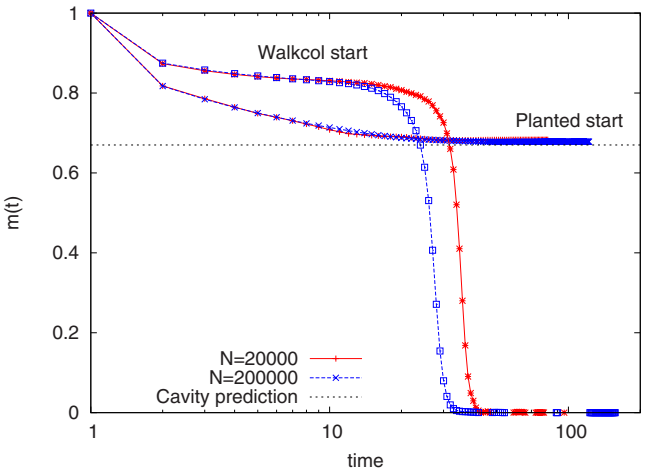

FIG. 15. (Color online) Iteration of belief propagation in the four-coloring problem of graph with average Poissonian degree $c=8.4$. The average magnetization of BP messages is plotted versus the number of iterations. When initialized in the equilibrium solution (obtained by planting), BP converge to the nontrivial magnetization, in agreement with the cavity prediction. On the very same graph, when initialized in a solution obtain by Walk-Col, it, however, converges to the trivial fixed point. This shows solutions found by heuristic solver are very different from the equilibrium ones, and instead belong to clusters that do not have an associated BP fixed point, as expected from the picture obtained by the following state method.

$T_e \to 0$ ($\epsilon \to 0$), the equations for the bottom energy of the states, Eqs. (68)–(71), reduce to the equations for frozen variables in the equilibrium zero-temperature states from Refs. 41 and 49.

In the same limit the bottom of a low T_e state, Eq. (72), is positive if there are frozen variables in the ground state $T_e=0$. Also in order to have a nontrivial (i.e., $E>0$) solution at finite T_e, we need a nontrivial solution at $T_e=0$: hence if there are no frozen variables in the ground state then Eqs. (68)–(71) have only the trivial paramagnetic solution for low T_e which means that either the bottoms of low T_e states are at zero energy *or* that we encountered again the previously discussed instability that prevents us to follow some states down to zero temperature using only the replica symmetric approach. On the other hand, when there are frozen variables in the equilibrium state at zero temperature the landscape is always valleys dominated and simulated annealing (and presumably any simple algorithm with local moves) will not be able to find the ground state: these correspond to truly difficult problems.

The instability toward RSB unfortunately prevents us from showing explicitly that the canyons-valleys transition is strictly larger than the dynamical transition (in the model such as K-SAT or graph coloring where the later does not coincide with the rigidity transition). However, it is reasonable to expect this is the case and indeed the behavior of simulated annealing observed in simulations confirms this.[42] The existence of a phase with canyon-dominated landscape thus explains the unreasonable efficiency of some stochastic local search algorithms.[63,92] The really hard problem requires the landscape not only to be glassy *but also* not to have states going down to zero energy with a large basins of attraction, i.e., to have a valleys-dominated energy landscape.

Our analysis also provides an insight about the types of solutions that are achieved by simulated annealing or stochastic local search. Those solutions are clearly not equilibrium ones and instead belong to the bottoms of states that undergo full-step replica symmetry breaking at low temperatures. The existence of the above-discussed spinodal line means that there is no low-temperature belief propagation fixed point associated to these states. This was indeed observed numerically in previous works[41,93,94]—when BP is initialized in a solution found by some heuristic algorithm it always converges back to the replica symmetric fixed point. The procedure called whitening[41,95–98] never finds a nontrivial fixed point either when initialized in solutions found by survey propagation or other heuristics.

Our results explicitly explain why solutions found by polynomial heuristics have quite different properties from the equilibrium solutions that are usually described by the cavity method. This shows how futile are the attempts to study clustering, BP fixed points, and other equilibrium predictions starting from solutions obtained by heuristics solvers. Instead exhaustive search, planting techniques, or other provably equilibrium procedures have to be used if one wants to consider equilibrium configurations.

In order to illustrate this we created an instance of the coloring problem using the quiet planting procedure and ran belief propagation initialized both in the planted configuration, and then in a solution found by the Walk-Col algorithm introduced in Ref. 41. Figure 15 shows how the magnetization evolves with the number of iterations. BP initialized in the planted configuration converges to a nontrivial fixed point at a value of magnetization that describes the *width* of the corresponding equilibrium states, which is perfectly in agreement with the cavity prediction.[41] However, BP initialized in the Walk-Col solution converges to a trivial fixed point after an intermediate plateau corresponding to flattening of the underlying potential. The potential does, however, not have a minimum hence BP ends up in the trivial fixed point.[99] This plateau corresponds to the deep minima found in experiments with whitening procedure, when the number of changes is plotted as a function of the number of interactions.[95,96] The same behavior is observed in the entropy at a certain distance from a solution investigated in Refs. 93 and 100, which is the Franz-Parisi potential at zero temperature. This show unambiguously that many types of solutions exist in these problems, and that one should not confuse the *equilibrium* thermodynamic solutions of the standard cavity approach, with the *out-of-equilibrium* solutions, that should be studied with the formalism we have introduced here.

VII. CONCLUSIONS AND DISCUSSION

We have described how to follow adiabatically Gibbs states in glassy mean-field models, answered some long-standing questions about the glassy energy landscape, and we have computed the residual energy after an adiabatically slow annealing from equilibrium. We have described the be-

havior of out-of-equilibrium states and demonstrated the presence of temperature chaos in these mean-field models. We have found interesting features of the energy landscape and identified a transition from a canyons-dominated landscape to a valleys-dominated one that allows to quantitatively understand why ground-state configurations are sometimes easy to find despite the presence of a glass transition. We have also shown that these out-of-equilibrium ground states have different properties than the equilibrium ones, thus explaining many apparent discrepancies between theory and simulations in the literature. Finally, we have also checked some of these results using Monte Carlo simulations.

On the methodological side of our work, the states following method we have developed has interesting connections to the reconstruction on trees and it is also closely related to the Franz-Parisi potential. In some models, it can be reinterpreted via the planting of an equilibrium configuration, which is, in particular, useful for speeding up simulations and we shall pursue on this aspect in forecoming works. A curious and interesting connection between the properties of the glassy systems and ferromagnets on the Nishimori line is found and its consequences for the physics of the glass transition will be also explored in subsequent works.

The method of states following has, however, one drawback that arises due to the instability of states toward full-step replica symmetry breaking at lower temperatures. Usually in such a situation a RS or 1RSB approach can be used as a sensible and very accurate approximation. However, we found ourselves here in the rather particular situation where there is *no* nonparamagnetic RS or 1RSB solution for states with T_e close to T_d at low T_a (as illustrated in Fig. 4), in a region where we anticipate FRSB to be the correct solution. Since it is not known how to obtain the FRSB solution in the diluted systems, this prevents us from computing concrete values of limiting energies for adiabatic simulated annealing initialized at high temperatures. Clearly this calls for new investigations and for new ways to approximate the FRSB solution. We have suggested one such approximation that gives a sensible solution even in this region in Sec. V G 2 but it is still a computationally costly one. A simpler approach thus needs to be developed. It would be, for instance, worth investigating if the supersymmetry broken cavity method (or the so-called two groups ansatz) (Refs. 101–103) could provide a nontrivial solution in the regions where the standard cavity method does not. The gap in the $\Sigma(s)$ (how many states of a given size are present) in the coloring problem reported in Ref. 41 might perhaps be related to the instability observed in the present paper.

The formalism of adiabatic evolution of states in temperature should extend straightforwardly when other external parameters are changed adiabatically. It would be interesting to see if one can take as the adiabatic external parameter the density of constraints (or average degree of the graph) one study the *connectivity* landscape introduced in Refs. 63 and 104. Our work offers extensions in many other directions, as detailed description of the complex energy landscape is immensely useful in understanding properties of complex glassy materials. Among possible applications are the studies of memory and rejuvenation protocols,[105] of jammed packings[12] and of the quantum adiabatic algorithm.[106,107]

ACKNOWLEDGMENTS

The authors would like to thank S. Franz, J. Kurchan, M. Mézard, G. Semerjian and D. Sherrington for very inspiring and useful discussions. We thank G. Semerjian, in particular, for thorough reading of the manuscript.

APPENDIX A: THE LARGE CONNECTIVITY LIMIT OF THE CAVITY EQUATIONS

The solution of the fully connected p-spin model was originally derived from the replica trick.[10,36–39] The cavity approach was developed later on as an alternative to the replica trick and the $p=2$ solution recovered in this way.[62] In this appendix, we remind how this computation generalizes and how the large connectivity limit of the cavity equations yields the RS and 1RSB solutions of the fully connected p-spin model. This should facilitate understanding of our derivation of the equations for states following in the main text.

1. Replica symmetric solution

To achieve our goal, it is first suitable to rewrite Eq. (4) in terms of cavity fields $h^{i\to a}$ and biases $u^{b\to i}$ defined as

$$\chi_s^{i\to a} = \frac{e^{\beta h^{i\to a} s}}{2\cosh \beta h^{i\to a}}, \tag{A1}$$

$$\psi_s^{b\to i} = \frac{e^{\beta u^{b\to i} s}}{2\cosh \beta u^{b\to i}}, \tag{A2}$$

it gives

$$h^{i\to a} = \sum_{b\in \partial i\backslash a} u^{b\to i}, \tag{A3}$$

$$\tanh(\beta u^{b\to i}) = \tanh(\beta J_b) \prod_{j\in \partial b\backslash i} \tanh(\beta h^{j\to b}). \tag{A4}$$

At this point, the recursion can thus be written in terms of the local fields $h^{i\to a}$ as

$$h^{i\to a} = \frac{1}{\beta} \sum_{b\in \partial i\backslash a} \operatorname{arctanh}\left[\tanh(\beta J_b) \prod_{j\in \partial b\backslash i} \tanh(\beta h^{j\to b})\right]. \tag{A5}$$

In the fully connected p-spin problem every spin is involved in $\binom{N-1}{p-1} \sim N^{p-1}/(p-1)!$ interactions, and each of these interactions J_b is small, of $O(N^{1-p})$. Equation (A5) can thus be rewritten introducing a new message $m^{i\to a} = \tanh(\beta h^{i\to a})$ as

$$m^{i\to a} = \tanh\left(\beta \sum_{b\in \partial i\backslash a} J_b \prod_{j\in \partial b\backslash i} m^{j\to b}\right) = \chi_1^{i\to a} - \chi_0^{i\to a}. \tag{A6}$$

At this point one realizes that the argument of the tanh is a sum of many terms. In the replica symmetric approximation

these terms are considered independent and thus according to the central limit theorem the sum is distributed as a Gaussian variable. We denote $m=\langle m^{i\to a}\rangle$ the mean (first moment) of $m^{i\to a}$ and $q=\langle (m^{i\to a})^2\rangle$ its second moment. Then the mean (first moment) of the sum in the argument of the tanh is $\mu=\beta J_0 p m^{p-1}$ and its variance $\sigma=\beta^2 J^2 p q^{p-1}/2$. Using the mean and variance we can write $m=\int e^{-(z-\mu)^2/(2\sigma)}\tanh z dz/\sqrt{2\pi\sigma}$ and $q=\int e^{-(z-\mu)^2/(2\sigma)}\tanh^2 z dz/\sqrt{2\pi\sigma}$, which after a substitution gives the usual form of the replica symmetric equation for the p-spin model, Eqs. (40) and (41), obtained in Ref. 37,

2. Free energy calculation

In the cavity formalism the RS free energy reads

$$-\beta F=\sum_i \log Z^{i+\partial i}-(p-1)\sum_a \log Z^a, \tag{A7}$$

where the free-energy shifts are

$$Z^{i+\partial i}=\sum_{s_i}\prod_{b\in\partial i}\sum_{s_{j\neq i}} e^{\beta J_b \prod_{j\in\partial b} s_j}\prod_{j\in\partial b\backslash i}\chi_{s_j}^{j\to b}, \tag{A8}$$

$$Z^a=\sum_{s_j} e^{\beta J_a \prod_{j\in\partial a} s_j}\prod_{j\in\partial a}\chi_{s_j}^{j\to a}. \tag{A9}$$

Let us now take the fully connected limit. The link term is (we write only the terms with J_b and J_b^2 as the rest in negligible)

$$\begin{aligned} Z^a&=\sum_{s_j}\left(1+\beta J_a\prod_{j\in\partial a} s_j+\frac{1}{2}\beta^2 J_a^2\right)\prod_{j\in\partial a}\chi_{s_j}^{j\to a}\\ &=1+\frac{1}{2}\beta^2 J_a^2+\beta J_a\prod_{j\in\partial a} m^{j\to a}. \end{aligned} \tag{A10}$$

Hence,

$$\begin{aligned} \sum_a \log Z^a&=\sum_a\left(\frac{1}{2}\beta^2 J_a^2+\beta J_a\prod_{j\in\partial a} m^{j\to a}\right.\\ &\quad\left.-\frac{1}{2}\beta^2 J_a^2\prod_{j\in\partial a}[m^{j\to a}]^2\right)\\ &=\frac{1}{4}\beta^2 J^2+\beta J m^p-\frac{1}{4}\beta^2 J^2 q^p. \end{aligned} \tag{A11}$$

The site term is a bit trickier. It is useful to remind the following relations:

$$\chi_s^{i\to a}=\frac{1+s m^{i\to a}}{2}=\frac{1+s\tanh\beta h^{i\to a}}{2}=\frac{e^{\beta h^{i\to a} s}}{2\cosh(\beta h^{i\to a})}. \tag{A12}$$

The site term can then be rewritten as

$$Z^{i+\partial i}=\sum_{s_i}\prod_{b\in\partial i}\sum_{s_{j\neq i}} e^{\beta J_b s_i \prod_{j\in\partial b\backslash i} s_j}\frac{e^{\beta\sum_j s_j h^{j\to b}}}{\prod_{j\in\partial b\backslash i} 2\cosh\beta h^{j\to b}}. \tag{A13}$$

Using trigonometric relation

$$\begin{aligned} \sum_{s_{j\neq i}} e^{\beta J_b s_i\prod_{j\in\partial b\backslash i} s_j} e^{\beta\sum_j s_j h^{j\to b}}&=\cosh\beta J_b s_i\prod_{j\in\partial b\backslash i} 2\cosh\beta h^{j\to b}\\ &\quad+\sinh\beta J_b s_i\prod_{j\in\partial b\backslash i} 2\sinh\beta h^{j\to b} \end{aligned} \tag{A14}$$

and odd/even properties of the sinh/cosh functions we have

$$\begin{aligned} Z^{i+\partial i}&=\sum_{s_i}\prod_{b\in\partial i}\left[2\cosh\beta J_b\frac{1+s_i\tanh\beta J_b\prod_{j\in\partial b\backslash i}\tanh\beta h^{j\to b}}{2}\right]. \end{aligned} \tag{A15}$$

Using relations (A4) and (A12) we get a useful form of the site term

$$Z^{i+\partial i}=2\cosh\left(\beta\sum_{b\in\partial i} u^{b\to i}\right)\prod_{b\in\partial i}\frac{\cosh\beta J_b}{\cosh\beta u^{b\to i}}. \tag{A16}$$

Only now we start developing the large connectivity limit in which interactions strengths are infinitesimal. Writing the site term in terms of messages $m^{b\to j}$ and expanding hyperbolic functions in the leading order we get

$$\begin{aligned} Z^{i+\partial i}&=2\cosh\left(\sum_{b\in\partial i}\beta J_b\prod_{j\in\partial b\backslash i} m^{j\to b}\right)\prod_{b\in\partial i}\frac{\cosh\beta J_b}{\cosh(\beta J_b\prod_{j\in\partial b\backslash i} m^{j\to a})} \end{aligned} \tag{A17}$$

$$\begin{aligned} &=2\cosh\left(\sum_{b\in\partial i}\beta J_b\prod_{j\in\partial b\backslash i} m^{j\to b}\right)\prod_{b\in\partial i}\left[1+\frac{\beta^2 J_b^2}{2}\right.\\ &\quad\left.-\frac{\beta^2 J_b^2}{2}\prod_{j\in\partial b\backslash i}(m^{j\to b})^2\right] \end{aligned} \tag{A18}$$

so that the site contribution to the free energy is

$$\begin{aligned} -\beta f^{i+\partial i}&=\int \mathcal{D}y\,\log 2\cosh(\beta J y\sqrt{p q^{p-1}/2}+\beta J_0 p m^{p-1})\\ &\quad+\frac{\beta^2 J^2 p}{4}(1-q^{p-1}). \end{aligned} \tag{A19}$$

Adding both terms together we get the replica symmetric free-energy density of the fully connected p-spin model,

$$\begin{aligned} -\beta f&=\frac{1}{4}\beta^2 J^2(p-1)q^p-\beta J_0(p-1)m^p+\frac{1}{4}\beta^2 J^2\\ &\quad-\frac{1}{4}\beta^2 J^2 p q^{p-1}+\int \mathcal{D}y\,\log 2\cosh(\beta J y\sqrt{p q^{p-1}/2}\\ &\quad+\beta J_0 p m^{p-1}). \end{aligned} \tag{A20}$$

3. 1RSB solution

To derive the infinite connectivity limit of the 1RSB cavity equations we define the mean and overlap parameters

$$m = \int \mathcal{D}Q(P) \left[\frac{\int dP(m^{i\to a}) Z(\{m^{i\to a}\},\beta)^x m^{i\to a}}{\int dP(m^{i\to a}) Z(\{m^{i\to a}\},\beta)^x} \right] \equiv \langle \langle m^{i\to a} \rangle_P \rangle_Q, \tag{A21}$$

$$q_1 = \int \mathcal{D}Q(P) \left[\frac{\int dP(m^{i\to a}) Z(\{m^{i\to a}\},\beta)^x (m^{i\to a})^2}{\int dP(m^{i\to a}) Z(\{m^{i\to a}\},\beta)^x} \right] \equiv \langle \langle (m^{i\to a})^2 \rangle_P \rangle_Q, \tag{A22}$$

$$q_0 = \int \mathcal{D}Q(P) \left[\frac{\int dP(m^{i\to a}) Z(\{m^{i\to a}\},\beta)^x m^{i\to a}}{\int dP(m^{i\to a}) Z(\{m^{i\to a}\},\beta)^x} \right]^2 \equiv \langle \langle m^{i\to a} \rangle_P^2 \rangle_Q, \tag{A23}$$

where the average over P is over the different states and average over Q is over the different edges in the graph. The message $m^{i\to a}$ is computed from the incoming messages according to Eq. (A6). The distribution $P(m^{i\to a})$ follows

$$P(m^{i\to a}) = \frac{1}{\mathcal{Z}} \int \prod_j P(m^{j\to b}) Z^{i\to a}[(m^{i\to a}),\beta]^x \delta\{m^{i\to a} - \mathcal{F}[(m^{j\to b}),\beta]\}, \tag{A24}$$

where the equations for $m^{i\to a} = \tanh(\beta X)$ are as in Eq. (A6), where

$$X = \sum_{b\in\partial i\backslash a} J_b \prod_{j\in\partial b\backslash i} m^{j\to b}. \tag{A25}$$

Note that the reweighting factor equals the site term, Eq. (A18), but only the part $\cosh(\beta X)$ is relevant, as the rest can be written as

$$e^{\sum_{b\in\partial i} \beta^2 J_b^2/2 [1 - \prod_{j\in\partial b\backslash i} (m^{j\to b})^2]} = e^{\beta^2 J^2 p/4 (1-q^{p-1})}, \tag{A26}$$

which is self-averaging and does not depend on the integration variables so it always cancels out as the reweighting appears in both the numerator and denominator.

The term X involves the sum random variables and it thus follows a bivariate Gaussian distribution that can be characterized by computing,

$$\mu \equiv \langle \langle X \rangle_P \rangle_Q = J_0 p m^{p-1}, \tag{A27}$$

$$\sigma_1 \equiv \langle \langle X^2 \rangle_P \rangle_Q - \langle \langle X \rangle_P \rangle_Q^2 = J^2 \frac{p}{2} q_1^{p-1}, \tag{A28}$$

$$\sigma_0 \equiv \langle \langle X \rangle_P^2 \rangle_Q - \langle \langle X \rangle_P \rangle_Q^2 = J^2 \frac{p}{2} q_0^{p-1}. \tag{A29}$$

At this point we are able to realize that the average over states $\langle \cdot \rangle_P$ can we written as an Gaussian integral of $\tanh X$ where the mean of X over states $\langle X \rangle_P$ and the variance $\sigma = \langle X^2 \rangle_P - \langle X \rangle_P^2$. The average over the graph $\langle \cdot \rangle_Q$ is also an average over a Gaussian variable with mean $\langle \langle X \rangle_P \rangle_Q = \mu$ and variance $\sigma_0 = \langle \langle X \rangle_P^2 \rangle_Q - \langle \langle X \rangle_P \rangle_Q^2$. Finally, $\langle \sigma \rangle_Q = \sigma_1 - \sigma_0$. All that gives averaged infinite connectivity 1RSB Eqs. (44)–(46). The parameter q_1 is the average self-overlap and q_0 the average overlap between states.

APPENDIX B: COMPUTING THE FRANZ-PARISI POTENTIAL IN DILUTED MODELS

We described the connection between the states following method and the Franz-Parisi potential. For completeness in this appendix, we give the equations according to which the Franz-Parisi potential is computed in the diluted (sparse) models.

The Franz-Parisi potential is the free energy $f(q)$ of the system at temperature β_a depend on the overlap q with an equilibrium configuration $\{\sigma_i\}$ at temperature β_e. In order to fix the overlap q we introduce a local uniform field h in the direction of the equilibrium configuration. Our goal is then to compute

$$f(h) = \frac{\sum_{\{\sigma_i\}} \tilde{f}(h,\{\sigma_i\}) e^{-\beta_e \mathcal{H}(\{\sigma_i\})}}{\sum_{\{\sigma_i\}} e^{-\beta_e \mathcal{H}(\{\sigma_i\})}}, \tag{B1}$$

$$e^{-\beta_a \tilde{f}(h,\{\sigma_i\})} = \sum_{\{s_i\}} e^{-\beta_a \mathcal{H}(\{s\}) + \beta_a h \sum_i s_i \sigma_i}. \tag{B2}$$

The Franz-Parisi potential is then

$$f(q) = f(h) + hq, \quad \frac{\partial f(h)}{\partial h} = -q. \tag{B3}$$

To obtain the value of $f(q)$ we need to solve equations similar to Eq. (27) where the field h is taken into account

$$\begin{aligned} \bar{\psi}_\sigma \bar{P}_\sigma(\psi|\bar{\psi}) \mathcal{P}_{\rm RS}(\bar{\psi}) = \sum_J Q(J) \sum_{\{l\}} q(\{l\}) \int \prod_{i=1}^{K-1} \prod_{j_i=1}^{l_i} & \times [d\bar{\psi}^{j_i} \mathcal{P}_{\rm RS}(\bar{\psi}^{j_i})] \delta[\bar{\psi} - \mathcal{F}(\{\bar{\psi}^{j_i}\},\beta_e)] \\ & \times \sum_{\{\sigma_i\}} e^{J\beta_e \sigma \Pi_i \sigma_i} \frac{\prod_{i=1}^{K-1} \prod_{j_i=1}^{l_i} \bar{\psi}^{j_i}_{\sigma_i}}{Z(\{\bar{\psi}^{j_i}\},\beta_e)} \\ & \times \int \prod_{i=1}^{K-1} \prod_{j_i=1}^{l_i} [d\psi^{j_i} \bar{P}^{j_i}_{\sigma_i}(\psi^{j_i}|\bar{\psi}^{j_i})] \delta[\psi - \mathcal{F}(\{\psi^{j_i}\},\beta_a,\{\sigma_i\},h)]. \end{aligned} \tag{B4}$$

where

$$\mathcal{F}_s(\{\psi^{j_i}\},\beta_a,\{\sigma_i\},h) = \psi_s = \sum_{\{s_i\}} \frac{e^{\beta_a J s \Pi_i s_i}}{Z(\{\psi^{j_i}\},\beta_a)} e^{\beta_a h \Sigma_i \sigma_i s_i} \prod_{i=1}^{K-1} \prod_{j_i=1}^{l_i} \psi^{j_i}_{s_i}. \tag{B5}$$

The free energy $f(h)$ is computed from the fixed point of Eq. (B4) as

$$-\beta_a f(h) = \alpha \sum_J Q(J) \sum_{\{l\}} q(\{l\}) \int \prod_{i=1}^{K} \prod_{j_i=1}^{l_i} [d\bar{\psi}^{j_i} \mathcal{P}_{\mathrm{RS}}(\bar{\psi}^{j_i})] \delta[\bar{\psi} - \mathcal{F}(\{\bar{\psi}^{j_i}\}, \beta_e)], \tag{B6}$$

$$\sum_{\{\sigma_i\}} e^{J\beta_e \prod_i \sigma_i} \frac{\prod_{i=1}^{K} \prod_{j_i=1}^{l_i} \bar{\psi}^{j_i}_{\sigma_i}}{Z^{a+\partial a}(\{\bar{\psi}^{j_i}\}, \beta_e)} \int \prod_{i=1}^{K} \prod_{j_i=1}^{l_i} [d\psi^{j_i} P^{j_i}_{\sigma_i}(\psi^{j_i})] \log Z^{a+\partial a}(\{\psi^j\}, \beta_a, \{\sigma_i\}, h)$$

$$-\sum_l \mathcal{Q}(l)(l-1) \int \prod_{i=1}^{l} [d\bar{\psi}^j \mathcal{P}_{\mathrm{RS}}(\bar{\psi}^j)] \frac{\sum_\sigma e^{\beta_e \sigma} \prod_{i=1}^{l} \bar{\psi}^j_\sigma}{Z^i(\{\bar{\psi}^j\}, \beta_e)} \int \prod_{i=1}^{l} [d\psi^j P^i_\sigma(\psi^j)] \log Z^i(\{\psi^j\}, \beta_a, \sigma, h) \tag{B7}$$

with the h-dependent partition function contributions being equal to

$$Z^{a+\partial a}(\{\psi^j\}, \beta_a, \{\sigma_i\}, h) = \sum_{\{s_i\}} e^{\beta_a J \prod_i s_i} e^{\beta_a h \sum_i \sigma_i s_i} \prod_{i=1}^{K} \prod_{j_i=1}^{l_i} \psi^{j_i}_{s_i}, \tag{B8}$$

$$Z^i(\{\psi^j\}, \beta_a, \sigma, h) = \sum_s e^{\beta_a s} e^{\beta_a h \sigma s} \prod_{i=1}^{l} \psi^j_s. \tag{B9}$$

The overlap is obtained by derivative with respect to h according to Eq. (B3). The nonconvex parts of $f(q)$ are computed by iteratively choosing a new value of h that gives the expected values of the overlap q in the same manner as total magnetization was fixed in Refs. 108 and 109.

Note that the states following method developed in this paper corresponds to the Franz-Parisi potential at $h=0$ initialized in the equilibrium configuration. In other words the states following is looking directly at the minimum of the Franz-Parisi potential that corresponds to the Gibbs state at temperature β_a.

[1] M. Born and V. A. Fock, Z. Phys. A: Hadrons Nucl. **51**, 165 (1928).
[2] L. F. Cugliandolo and J. Kurchan, Phys. Rev. Lett. **71**, 173 (1993).
[3] A. Barrat, S. Franz, and G. Parisi, J. Phys. A **30**, 5593 (1997).
[4] A. V. Lopatin and L. B. Ioffe, Phys. Rev. B **66**, 174202 (2002).
[5] A. Montanari and F. Ricci-Tersenghi, Phys. Rev. B **70**, 134406 (2004).
[6] F. Krzakala and O. C. Martin, Eur. Phys. J. B **28**, 199 (2002).
[7] B. Capone, T. Castellani, I. Giardina, and F. Ricci-Tersenghi, Phys. Rev. B **74**, 144301 (2006).
[8] T. Rizzo and H. Yoshino, Phys. Rev. B **73**, 064416 (2006).
[9] T. Mora and L. Zdeborová, J. Stat. Phys. **131**, 1121 (2008).
[10] T. R. Kirkpatrick and D. Thirumalai, Phys. Rev. Lett. **58**, 2091 (1987).
[11] M. Mézard and G. Parisi, Phys. Rev. Lett. **82**, 747 (1999).
[12] G. Parisi and F. Zamponi, Rev. Mod. Phys. **82**, 789 (2010).
[13] E. Shakhnovich and A. M. Gutin, J. Phys. A **22**, 1647 (1989).
[14] L. Ioffe and M. Mézard, arXiv:0909.2263 (unpublished).
[15] M. Mézard, G. Parisi, and M. A. Virasoro, *Spin-Glass Theory and Beyond*, Lecture Notes in Physics Vol. 9 (World Scientific, Singapore, 1987).
[16] M. Mézard, G. Parisi, and R. Zecchina, Science **297**, 812 (2002).
[17] F. Krzakala, A. Montanari, F. Ricci-Tersenghi, G. Semerjian, and L. Zdeborová, Proc. Natl. Acad. Sci. U.S.A. **104**, 10318 (2007).
[18] M. Mézard and A. Montanari, *Physics, Information, Computation* (Oxford University Press, Oxford, 2009).
[19] M. Mézard and G. Parisi, Eur. Phys. J. B **20**, 217 (2001).
[20] J.-P. Bouchaud, L. Cugliandolo, J. Kurchan, and M. Mézard, in *Spin Glasses and Random Fields*, edited by A. P. Young (World Scientific, Singapore, 1998).
[21] A. Montanari and G. Semerjian, J. Stat. Phys. **124**, 103 (2006).
[22] W. Kauzmann, Chem. Rev. **43**, 219 (1948).
[23] E. Gardner, Nucl. Phys. B **257**, 747 (1985).
[24] A. Montanari and G. Semerjian, J. Stat. Phys. **125**, 23 (2006).
[25] F. Krzakala and L. Zdeborová, arXiv:0909.3820 (unpublished).
[26] M. Mézard and A. Montanari, J. Stat. Phys. **124**, 1317 (2006).
[27] S. Franz and G. Parisi, J. Phys. I **5**, 1401 (1995).
[28] S. Franz and G. Parisi, Phys. Rev. Lett. **79**, 2486 (1997).
[29] H. Nishimori, Prog. Theor. Phys. **66**, 1169 (1981).
[30] F. Ricci-Tersenghi, M. Weigt, and R. Zecchina, Phys. Rev. E **63**, 026702 (2001).
[31] M. Mézard, F. Ricci-Tersenghi, and R. Zecchina, J. Stat. Phys. **111**, 505 (2003).
[32] S. Franz, M. Mézard, F. Ricci-Tersenghi, M. Weigt, and R. Zecchina, Europhys. Lett. **55**, 465 (2001).
[33] S. Cocco, O. Dubois, J. Mandler, and R. Monasson, Phys. Rev. Lett. **90**, 047205 (2003).
[34] R. G. Gallager, IEEE Trans. Inf. Theory **8**, 21 (1962).
[35] D. J. C. MacKay, IEEE Trans. Inf. Theory **45**, 399 (1999).
[36] B. Derrida, Phys. Rev. Lett. **45**, 79 (1980).
[37] D. Gross and M. Mézard, Nucl. Phys. B **240**, 431 (1984).
[38] T. R. Kirkpatrick and D. Thirumalai, Phys. Rev. B **36**, 5388 (1987).
[39] T. R. Kirkpatrick, D. Thirumalai, and P. G. Wolynes, Phys. Rev.

A **40**, 1045 (1989).
[40] H. A. Bethe, Proc. R. Soc. London, Ser. A **150**, 552 (1935).
[41] L. Zdeborová and F. Krząkała, Phys. Rev. E **76**, 031131 (2007).
[42] J. van Mourik and D. Saad, Phys. Rev. E **66**, 056120 (2002).
[43] R. Mulet, A. Pagnani, M. Weigt, and R. Zecchina, Phys. Rev. Lett. **89**, 268701 (2002).
[44] A. Braunstein, R. Mulet, A. Pagnani, M. Weigt, and R. Zecchina, Phys. Rev. E **68**, 036702 (2003).
[45] F. Krząkała, A. Pagnani, and M. Weigt, Phys. Rev. E **70**, 046705 (2004).
[46] F. Krząkała and L. Zdeborová, EPL **81**, 57005 (2008).
[47] F. Krzakala and L. Zdeborová, Phys. Rev. Lett. **102**, 238701 (2009).
[48] L. Zdeborová and F. Krzakala, arXiv:0902.4185 (unpublished).
[49] G. Semerjian, J. Stat. Phys. **130**, 251 (2008).
[50] L. Zdeborová, Acta Phys. Slov. **59** (3), 169 (2009).
[51] A. Montanari, F. Ricci-Tersenghi, and G. Semerjian, J. Stat. Mech.: Theory Exp. (2008), P04004.
[52] A. Montanari, F. Ricci-Tersenghi, and G. Semerjian, in *45th Allerton Conference on Communications, Control and Computing*, Monticello, Illinois, arXiv:0709.1667.
[53] F. Ricci-Tersenghi and G. Semerjian, J. Stat. Mech.: Theory Exp. (2009), P09001.
[54] A. Sly, Commun. Math. Phys. **288**, 943 (2009).
[55] D. Achlioptas and A. Coja-Oghlan, in *Proceedings of the 2008 49th Annual IEEE Symposium on Foundations of Computer Science*, (IEEE Computer Society, Washington D.C., 2008), pp. 793-802, http://portal.acm.org/citation.cfm?id=1470582.1470627
[56] H. Nishimori, *Statistical Physics of Spin Glasses and Information Processing: An Introduction* (Oxford University Press, Oxford, UK, 2001).
[57] H. Nishimori and K. Y. M. Wong, Phys. Rev. E **60**, 132 (1999).
[58] H. Nishimori and M. J. Stephen, Phys. Rev. B **27**, 5644 (1983).
[59] F. Krzakala and L. Zdeborová (unpublished).
[60] A. Montanari, G. Parisi, and F. Ricci-Tersenghi, J. Phys. A **37**, 2073 (2004).
[61] M. Mézard, G. Parisi, and M. A. Virasoro, J. Phys. (France) Lett. **46**, 217 (1985).
[62] M. Mézard, G. Parisi, and M. A. Virasoro, Europhys. Lett. **1**, 77 (1986).
[63] F. Krzakala and J. Kurchan, Phys. Rev. E **76**, 021122 (2007).
[64] R. Mari, F. Krzakala, and J. Kurchan, Phys. Rev. Lett. **103**, 025701 (2009).
[65] A. Montanari and F. Ricci-Tersenghi, Eur. Phys. J. B **33**, 339 (2003).
[66] A. Crisanti, L. Leuzzi, and T. Rizzo, Phys. Rev. B **71**, 094202 (2005).
[67] D. S. Fisher and D. A. Huse, Phys. Rev. Lett. **56**, 1601 (1986).
[68] A. J. Bray and M. A. Moore, Phys. Rev. Lett. **58**, 57 (1987).
[69] J. R. Banavar and A. J. Bray, Phys. Rev. B **35**, 8888 (1987).
[70] I. Kondor, J. Phys. A **22**, L163 (1989).
[71] S. Franz and M. Ney-Nifle, J. Phys. A **28**, 2499 (1995).
[72] M. Sasaki and K. Nemoto, J. Phys. Soc. Jpn. **69**, 2283 (2000).
[73] P. E. Jönsson, H. Yoshino, and P. Nordblad, Phys. Rev. Lett. **89**, 097201 (2002).
[74] R. Mulet, A. Pagnani, and G. Parisi, Phys. Rev. B **63**, 184438 (2001).
[75] T. Rizzo, J. Phys. A **34**, 5531 (2001).
[76] A. Billoire and E. Marinari, J. Phys. A **33**, L265 (2000).
[77] T. Aspelmeier, A. J. Bray, and M. A. Moore, Phys. Rev. Lett. **89**, 197202 (2002).
[78] T. Rizzo and A. Crisanti, Phys. Rev. Lett. **90**, 137201 (2003).
[79] M. Sasaki and O. C. Martin, Europhys. Lett. **60**, 316 (2002).
[80] H. G. Katzgraber and F. Krzakała, Phys. Rev. Lett. **98**, 017201 (2007).
[81] D. Sherrington and S. Kirkpatrick, Phys. Rev. Lett. **35**, 1792 (1975).
[82] M. Gabay and G. Toulouse, Phys. Rev. Lett. **47**, 201 (1981).
[83] C. Kwon and D. J. Thouless, Phys. Rev. B **37**, 7649 (1988).
[84] T. Castellani, F. Krzakala, and F. Ricci-Tersenghi, Eur. Phys. J. B **47**, 99 (2005).
[85] H. N. P. Gillin and D. Sherrington, J. Phys. A **34**, 2949 (2001).
[86] M. Hasenbusch, A. Pelissetto, and E. Vicari, Phys. Rev. B **78**, 214205 (2008).
[87] S. Franz, G. Parisi, and M. A. Virasoro, J. Phys. I **2**, 1869 (1992).
[88] S. Franz and G. Parisi, Physica A **261**, 317 (1998).
[89] H. Sompolinsky and A. Zippelius, Phys. Rev. Lett. **47**, 359 (1981).
[90] H. Sompolinsky and A. Zippelius, Phys. Rev. B **25**, 6860 (1982).
[91] L. F. Cugliandolo and J. Kurchan, J. Phys. A **27**, 5749 (1994).
[92] J. Ardelius and E. Aurell, Phys. Rev. E **74**, 037702 (2006).
[93] L. Dall'Asta, A. Ramezanpour, and R. Zecchina, Phys. Rev. E **77**, 031118 (2008).
[94] K. Li, H. Ma, and H. Zhou, Phys. Rev. E **79**, 031102 (2009).
[95] G. Parisi, arXiv:cs/0301015 (unpublished).
[96] E. N. Maneva, E. Mossel, and M. J. Wainwright, J. ACM **54**, article 17 (2007).
[97] A. Braunstein and R. Zecchina, J. Stat. Mech.: Theory Exp. **2004**, P06007 (2004).
[98] S. Seitz, M. Alava, and P. Orponen, J. Stat. Mech.: Theory Exp. **2005**, P06006 (2005).
[99] Interestingly the magnetization of the plateau is higher than the equilibrium magnetization, suggesting that clusters found by heuristic solves are smaller than the equilibrium ones, this is somewhat counterintuitive and requires further investigation.
[100] H. Zhou, arXiv:0911.4328 (unpublished).
[101] T. Rizzo, J. Phys. A **38**, 3287 (2005).
[102] A. Cavagna, I. Giardina, and G. Parisi, Phys. Rev. B **71**, 024422 (2005).
[103] M. Müller, L. Leuzzi, and A. Crisanti, Phys. Rev. B **74**, 134431 (2006).
[104] At this point we want to mention that we tried to do this and obtained equations identical to those in Sec. VI C. This however predicts a duality between the value of c_d and T_d which does not hold. It is yet to be understood if this prediction fails due to the FRSB instability or due to another effect to be discovered.
[105] V. Dupuis, E. Vincent, J.-P. Bouchaud, J. Hammann, A. Ito, and H. A. Katori, Phys. Rev. B **64**, 174204 (2001).
[106] T. Kadowaki and H. Nishimori, Phys. Rev. E **58**, 5355 (1998).
[107] E. Farhi, J. Goldstone, S. Gutmann, and M. Sipser, arXiv:quant-ph/0001106 (unpublished).
[108] F. Krzakala, F. Ricci-Tersenghi, and L. Zdeborová, Phys. Rev. Lett. **104**, 207208 (2010).
[109] P. Šulc and L. Zdeborová, arXiv:0912.3563, J. Phys. A: Math. Theor. (to be published).